



# Generator Level Study of the Decay

$$B_s^0 \longrightarrow J/\psi \phi \longrightarrow \mu^+ \mu^- K^+ K^-$$



Muhammad Ahmad

Department of Physics  
Quaid-i-Azam University  
Islamabad 45320  
Pakistan

June 16, 2007

This work is submitted as a dissertation  
in partial fulfilment of  
the requirement for the degree of

**MASTER OF PHILOSOPHY**  
in  
**PHYSICS**

Department of Physics  
Quaid-i-Azam University  
Islamabad 45320  
Pakistan

# Certificate

It is certified that the work contained in this dissertation was carried out by Mr. Muhammad Ahmad under my supervision.



Prof. Dr. Riazuddin

Supervisor

National Center for Physics

Quaid-i-Azam University

Islamabad 45320

Pakistan

Submitted through:



Prof. Dr. Pervez Hoodbhoy

Chairman

Department of Physics

Quaid-i-Azam University

Islamabad 45320

Pakistan

# Acknowledgements


In the name of ALLAH, the Most Merciful, Most Gracious, and Benevolent. My thanks would be incomplete without mentioning the Prophet Muhammad(PBUH), Who always encouraged people to Explore the Nature. I think the main credit of my studies goes to my grand Father, Who had spent his life in educating and giving awareness to his village people. I like to say about my father here that he is a Great man. He provided me the opportunity for higher studies and provided me all financial and moral support.

Then I would like to thank my supervisor Prof. Riazuddin for his great support and encouraging behavior which gave me confidence to work in particle physics. I would like to thank Prof. Hafeez Hoorani for guiding, correcting and encouraging me at all stages of my research and introducing me to the field of experiment particle physics very impressively. I would also like to thank Prof. Faheem Hussain for his cooperation and a very nice company from which I learned a lot. I would never forget to thank my school teacher Sir. Mateen Najmi who gave me the first and great motivation to come in the field of physics by telling me always "Bohat Physics Aati hay Bhi Aap ko". Thanks to my school teacher Sir. Amir Sajaad for helping me a lot in my studies and Prof. Ashghar Hashmi who encouraged me for higher studies.

My heartiest thanks to all my friends especially Jamil, Shabbar, Ishtiaq, Asif, Ali, Jamal, Ghouri, Ali Rai, Waqar, Zulqarnain, Jahanzaib, Nadeem, Mahmood, Shakeel, Hafiz Ishtiaq, Hammad and Kamran. Their warm companionship made the life at campus beautiful and unforgettable. I also remember my city friends Waseem, Zahid, Sajid and Saadat for their great time with me. I like to thank my group members Taimoor, Hamid, Ijaz, Irfan and Madam Shamoona for their fruitful discussion and nice company. I have no words to thank Madam Jamila for her great support and

encouragement whenever I lost my patience and hope throughout the work.

Finally, I wish to record my deepest obligation to my Mother for her love and care. I also want to mention my Brothers and specially sisters, who always prayed for my better future. Especially I want to mention Farooq who is my Friend more than a brother. The innocent smile childlike of my nieces Marfoa, Kainaat, Nidaal and nephew Shahzaib made the world beautiful as heaven . A great thanks to my family for their unconditional support, belief in me and for keeping me grounded.

  
Muhammad Ahmad

# Abstract

The LHC at CERN will be the largest  $b$ -factory ever built. The decay  $B_s^0 \rightarrow J/\psi \phi \rightarrow \mu^+ \mu^- K^+ K^-$  is chosen as a benchmark channel since it is representative of exclusive B physics studies. In this dissertation, we performed the generator level study of the channel  $B_s^0 \rightarrow J/\psi \phi \rightarrow \mu^+ \mu^- K^+ K^-$  at CMS using a specialized  $b\bar{b}$  generator called SIMUB and using BtoVVana for Root analysis. The generator level distributions of 120000 events of  $B_s^0 \rightarrow J/\psi \phi \rightarrow \mu^+ \mu^- K^+ K^-$  were studied, in particular their helicity angle distributions which were not possible to be studied using only PYTHIA, QQ and CMSSW. Hence they are usefull for the analysis of real data when the detector will become operational.

*To My Father and Grand Father Ustaad Khair  
Muhammad Khan Abbasi(Late).*

# Table of Contents

Table of Contents	v
List of Tables	viii
List of Figures	ix
Abstract	xi
Acknowledgements	xii
<b>1 Standard Model and B Physics</b>	<b>1</b>
1.1 Introduction . . . . .	1
1.2 Elementary Particles . . . . .	2
1.2.1 Fermions . . . . .	2
1.2.2 Mediator Particles . . . . .	3
1.3 Fundamental Forces . . . . .	4
1.4 Symmetries in the Standard Model . . . . .	5
1.4.1 Gauge Theories . . . . .	6
1.5 CP Violation . . . . .	7
1.5.1 Cabbibo Kobayashi Maskawa (CKM) Matrix . . . . .	8
1.6 B Physics . . . . .	9
1.6.1 Bottom Quark . . . . .	9
1.6.2 Production of $B_s^0$ Mesons at Hadron Colliders . . . . .	10
1.6.3 The $B_s^0 \rightarrow J/\psi \phi \rightarrow \mu^+ \mu^- K^+ K^-$ Decay at CMS . . . . .	12
1.6.4 Angular Analysis . . . . .	16
<b>2 The CMS Experiment at LHC</b>	<b>19</b>
2.1 The Large Hadron Collider at CERN . . . . .	19
2.1.1 The Accelerator . . . . .	19



2.1.2	Main Goals of LHC . . . . .	24
2.2	The CMS Detector . . . . .	24
2.2.1	General layout of CMS . . . . .	25
2.3	Geometry of CMS . . . . .	27
2.3.1	The Magnet . . . . .	27
2.3.2	The Tracker . . . . .	28
2.3.3	The Electromagnetic Calorimeter (ECAL) . . . . .	29
2.3.4	The Hadron Calorimeter . . . . .	30
2.3.5	The Muon System . . . . .	31
2.3.6	The Trigger system . . . . .	33
2.3.7	CMS Physics Motivation . . . . .	34
<b>3</b>	<b>Software Package</b>	<b>37</b>
3.1	Introduction . . . . .	37
3.2	General structure of program SIMUB . . . . .	39
3.3	Event Generation . . . . .	40
3.3.1	Generation of $b\bar{b}$ in <code>bb_gen</code> . . . . .	40
3.3.2	b-quark Fragmentation into $B_s^0$ in <code>bb_frg</code> . . . . .	42
3.3.3	$B_s^0$ decay and Analysis in <code>BB_dec</code> . . . . .	43
3.3.4	<code>BtoVVana</code> . . . . .	44
3.3.5	Preparation of input files by the SIMUB generator . . . . .	45
3.4	ROOT . . . . .	46
3.5	Lorentz Transformation . . . . .	48
<b>4</b>	<b>Results and Discussion</b>	<b>50</b>
4.1	Invariant Mass . . . . .	50
4.2	Opening Angle . . . . .	51
4.3	Total Momentum . . . . .	53
4.4	Transverse Momentum . . . . .	55
4.4.1	Transverse Momentum of $B_s^0$ , $J/\psi$ and $\phi$ . . . . .	56
4.4.2	Transverse Momentum of $\mu^+$ , $\mu^-$ , $K^+$ and $K^-$ . . . . .	57
4.5	Total Energy . . . . .	57
4.6	Transverse Energy . . . . .	59
4.7	Pseudorapidity . . . . .	61
4.7.1	Pseudorapidity of $B_s$ , $J/\psi$ , $\phi$ . . . . .	62
4.7.2	Pseudorapidity of $\mu^+$ , $\mu^-$ . . . . .	63
4.7.3	Pseudorapidity of $K^+$ , $K^-$ . . . . .	64
4.8	Polar Angle . . . . .	65
4.9	Boost . . . . .	66

4.10 Helicity Angles . . . . .	68
4.10.1 Distribution of $\text{Cos } \Theta_{\mu^+}$ . . . . .	68
4.10.2 Distribution of $\text{Cos } \Theta_{K^+}$ . . . . .	69
4.10.3 Distribution of $\chi$ . . . . .	70
<b>Conclusion</b>	<b>72</b>
<b>Bibliography</b>	<b>73</b>

# List of Tables

1.1	List of Elementary Particles (Leptons and Quarks). . . . .	4
1.2	List of Four Basic Forces. . . . .	5
1.3	The bb-pair production at LHC and other accelerators. . . . .	10
1.4	The number of $B_s^0 \rightarrow J/\psi\phi \rightarrow \mu^+\mu^-K^+K^-$ Events produced per year at CMS. . . . .	15
2.1	Technical properties of the Large Hadron Collider at CERN, relevant to the pp high luminosity mode. . . . .	23
4.1	Values of pseudorapidity corresponding to polar angle $\theta$ . . . . .	62

# List of Figures

1.1	Some of the leading order diagrams, describing heavy-flavour production in hadron collisions. . . . .	11
1.2	colour suppressed diagram for $B_s^0 \rightarrow J/\psi\phi$ . . . . .	13
1.3	Defination of three angles $\Theta_{l^+}$ , $\Theta_{l^-}$ , $\chi_{l^+}$ , describing the kinematics of the $B_s^0 \rightarrow J/\psi\phi$ decay chain in the helicity frame of reference. . . . .	17
2.1	Overview of LHC with four main detectors. . . . .	21
2.2	General layout of the CMS detector at the Large Hadron Collider at CERN. . . . .	27
3.1	The flow of data within the package SIMUB. . . . .	39
4.1	Invariant Mass of $B_s^0$ , $J/\psi$ and $\phi$ . . . . .	51
4.2	Opening Angle of $B_s^0$ , $J/\psi$ and $\phi$ . . . . .	52
4.3	Total Momentum of $B_s^0$ , $J/\psi$ and $\phi$ . . . . .	53
4.4	Total Momentum of $\mu^+$ , $\mu^-$ , $K^+$ and $K^-$ . . . . .	54
4.5	Transverse Momentum of $B_s^0$ , $J/\psi$ and $\phi$ . . . . .	55
4.6	Transverse Momentum of $\mu^+$ , $\mu^-$ , $K^+$ and $K^-$ . . . . .	56
4.7	Total Energy of $B_s^0$ , $J/\psi$ and $\phi$ . . . . .	58
4.8	Total Energy of $\mu^+$ , $\mu^-$ , $K^+$ and $K^-$ . . . . .	59
4.9	Transverse Energy of $B_s^0$ , $J/\psi$ and $\phi$ . . . . .	60
4.10	Transverse Energy of $\mu^+$ , $\mu^-$ , $K^+$ and $K^-$ . . . . .	61
4.11	Pseudorapidity of $B_s^0$ , $J/\psi$ and $\phi$ . . . . .	63

4.12	Pseudorapidity of $\mu^+, \mu^-, K^+$ and $K^-$ . . . . .	64
4.13	Polar Angle of $B_s^0, J/\psi$ and $\phi$ . . . . .	65
4.14	Polar Angle of $\mu^+, \mu^-, K^+$ and $K^-$ . . . . .	66
4.15	Boost of $B_s^0, J/\psi$ and $\phi$ . . . . .	67
4.16	Boost of $\mu^+, \mu^-, K^+$ and $K^-$ . . . . .	68
4.17	Distribution of $\text{Cos } \Theta_{\mu^+}$ . . . . .	69
4.18	Distribution of $\text{Cos } \Theta_{K^+}$ . . . . .	70
4.19	Distribution of $\chi$ . . . . .	71

# Chapter 1

## Standard Model and B Physics

### 1.1 Introduction

The universe around us is full of diverse physical and non-physical objects both seen and unseen by naked eye. Man is curious animal and he has been asking questions and seeking answers throughout the course of history starting from Aristotle and Socrates; are all the bewildering variety of objects seen in nature, made up of some elementary particles? If so how many elementary particles there are and how do they coalesce to form all the physical objects seen around us. Particle Physics is a basic science that deals with answering these questions that mankind has been asking for at least the last 5000 years. It is only in the last four decades that we have seen a reasonable progress towards understanding ourselves and the world around us.

Our greatest endeavor in basic science, undoubtedly, has been the study of matter and its constituent particles. Now strengthening the arena of basic scientific research, the greatest synthesis of all time which describes the basic interactions of all the particles, has been achieved in the form of the standard Model of Particle physics. Elementary particles can be classified into two major groups; the fermions with spin

$\frac{1}{2}$  and the bosons with spin 1.

## 1.2 Elementary Particles

High energy particle physics is basic science that aims to find out the fundamental constituents of matter. This quest has an evolving scheme throughout the history of mankind. Starting when people considered fire, water, earth and air as fundamental to when the atom was considered basic. These days we have the quarks and leptons as matter particles tomorrow may be something else.

### 1.2.1 Fermions

The fermions are the fundamental particles with half-integral spin and they obey the Pauli Exclusion Principle. There are two types elementary fermions: quarks and leptons (see Table 1.1).

#### Leptons

Leptons are fundamental particles with half-integral spin that does not feel the strong nuclear force. There are three known types or flavors of leptons: the electron, the muon, and the tau. Each flavor is represented by a pair of particles called a weak doublet, one of which is a massive charged particle (like the electron) and the other is a nearly massless neutral particle called a neutrino (such as the electron neutrino). The charged leptons have two possible spin states, while only one helicity is observed for the neutrinos (all the neutrinos are left-handed, and all the antineutrinos are right-handed).

## Quarks

Quarks are elementary particles with half-integral spin but they are the only one that interact through all four of the fundamental forces. Quarks come in six types or flavors and are named up (u), down (d), charm (c), strange(s), top (t) and bottom (b). Antiparticles of quarks are called antiquarks. Quarks are not found as independent entities on nature. They are always found as combination of quark antiquark ( $q\bar{q}$ ) pair states called mesons or groups of three quarks ( $qqq$ ) called baryons. These combinations of quarks either a meson or baryon is called a hadron. Three same flavored quarks with half-integral spin in a baryon lead to a contradiction with the Pauli Exclusion Principle and the Fermi-Dirac statistics for systems composed of identical fermions. The Pauli Exclusion Principle states that in the baryon ( $qqq$ ) state, the three valence quarks can only be formed in the antisymmetric final state. To satisfy this requirement physicist came up with the idea of an internal quantum number called “color”. The color of each quark in a baryon is such that it makes the combination  $qqq$  an antisymmetric state. There are three different types of color named after three basic colors red (r), blue (b) and green (g). The mesons and baryons are color neutral or color singlet.

### 1.2.2 Mediator Particles

Fermions interact with each other with mediator particles. The mediators are spin 1 vector bosons. These are photon, gluon,  $W^+$ ,  $W^-$  and  $Z_0$  boson. The photon ( $\gamma$ ) is responsible for electromagnetic interaction,  $W^+$ ,  $W^-$  and  $Z_0$  bosons take part in weak interaction and gluons (g) are responsible for strong interaction. The photon and gluon are massless and chargeless particles however the mass of  $W^+$ ,  $W^-$  is



$80.39\text{GeV}/c^2$  and  $Z_0$  has a mass of  $91.188\text{GeV}/c^2$  as shown in the Table 1.2.

Table 1.1: List of Elementary Particles (Leptons and Quarks).

FERMIONS					
Leptons spin ( $\frac{1}{2}$ )			Quarks spin ( $\frac{1}{2}$ )		
Flavour	Mass $\text{GeV}/c^2$	Electric Charge	Flavour	Approx. Mass $\text{GeV}/c^2$	Electric Charge
Electron neutrino ( $\nu_e$ )	$(0-0.13)\times 10^{-9}$	0	up (u)	0.002	$\frac{2}{3}$
Electron (e)	0.000511	-1	down (d)	0.005	$-\frac{1}{3}$
Muon neutrino ( $\nu_\mu$ )	$(0.009-0.13)\times 10^{-9}$	0	charm (c)	1.3	$\frac{2}{3}$
Muon ( $\mu$ )	0.106	-1	strange (s)	0.1	$-\frac{1}{3}$
Tau neutrino ( $\nu_\tau$ )	$(0.04-0.14)\times 10^{-9}$	0	top (t)	173	$\frac{2}{3}$
Tau ( $\tau$ )	1.777	-1	bottom (b)	4.2	$-\frac{1}{3}$

### 1.3 Fundamental Forces

There are four basic forces that enable the interactions between particles, electromagnetic, weak, strong and gravitational force. An interaction between two particles is defined as the exchange of mediating particle (see Table 1.2). The Strong Force, being the strongest of all, causes the interaction between quarks that holds them together in hadrons. It is mediated by 8 kinds of gluons that exchange the quantum number called 'color' between the quarks. Leptons can not interact strongly as they do not have color quantum number. Electromagnetic force which causes the electromagnetic

interactions between the charged particles, is mediated by photons. Weak Force which is responsible for the weak interaction between the particles, is mediated by the  $W^+$ ,  $W^-$  and  $Z_0$  bosons. Weak interaction changes one quark flavor to the other. Weak interaction can occur between quarks and leptons because it color independent. The range of weak force as predicted by the uncertainty principle is 10-18m whereas the range of strong force is 10-15m. Neutrinos have no charge and do not experience electromagnetic force but they do participate in weak interaction.

Gravitational Force, presumed to be mediated by the graviton, is still unknown to us. Gravitational force is ignored in the picture of high energy physics as it is an order of 30 magnitudes smaller than weak force.

Table 1.2: List of Four Basic Forces.

Force	Gauge Boson	Mass	Charge	Range(m)	Relative Strength
Strong	8 gluons	0	0	$10^{-15}$	$10^{38}$
Electromagnetic	Photon	0	0	infinite	$10^{36}$
Weak	W, Z bosons	81, 92GeV	$\pm 1, 0$	$10^{-18}$	$10^{25}$
Gravitational	Graviton	0	0	infinite	1

## 1.4 Symmetries in the Standard Model

Symmetries, as wide or as narrow as you may define its meaning, is one idea by which man through ages has tried to comprehend and create order, beauty and perfection. The concept of symmetry has been of ever increasing importance in fundamental theoretical physics. Therefore, in determining the dynamical structure of Standard Model (SM), symmetry is advised as its foundation stone.

### 1.4.1 Gauge Theories

Particles and their interactions are described by gauge theories, a special class of quantum theories which are invariant under Lorentz transformation. The invariance principle implies the existence of interactions that are mediated by gauge bosons. Gauge theories involve two kinds of particles; ones that carry charge and others that mediate interaction that are mediated by gauge bosons. The particles that carry charge are the fundamental fermions and non-abelian gauge boson, whereas the particles mediating interactions consists solely of gauge bosons, both abelian and non-abelian. The abelian gauge bosons do not interact with each other while the non-abelian gauge bosons interact with each other.

To date, three of the observed forces of nature have been successfully described in terms of gauge symmetries and these forces can be described in terms of unitary groups of different dimensions. Physicist describe combinations of gauge groups as  $SU(3)_C \times SU(2)_L \times U(1)_Y$ . There are  $(N^2 - 1)$  gauge bosons in the gauge theory described by the groups  $SU(N)$ . The group  $SU(3)_C$  describes strong interaction known as quantum chromodynamics (QCD). The gauge field of this theory is the gluon which is massless. The group  $SU(3)_C$  has 8 generators as predicted by the theory. The group  $SU(2)$  describes the weak interactions. It has three generators which correspond to  $W^+$ ,  $W^-$  and  $Z_0$ . This theory describes the interaction of only left handed particles. For left handed particle the spin and momentum are anti-parallel.

The theory describing the electrodynamic interaction is quantum electrodynamics (QED). It is constructed by applying the principle of local gauge invariance to the free Dirac Lagrangian. The corresponding operator  $U = e^{iH}$  belongs to abelian group  $U(1)_Y$ , where the gauge  $H$  is just a real number. To construct the locally invariant

transforms a left-handed neutrino into a right-handed anti-neutrino, which does exist.

If CP were an exact symmetry, the laws of Nature would be the same for matter and antimatter. We observe that most phenomena are C- and P-symmetric, and therefore, also CP-symmetric. In particular, these symmetries are respected by the electromagnetic, and strong interactions. While weak interactions violate C and P separately, CP is still preserved in most weak interaction processes. The CP symmetry is, however, violated in certain rare processes, as discovered in neutral K decays in 1964 [1], and recently observed in neutral B decays.

There are three different types of CP violation in meson decays:

1. CP violation in mixing, which occurs when the two neutral mass eigenstate admixtures cannot be chosen to be CP-eigenstates.
2. CP violation in decay, which occurs in both charged and neutral decays, when the amplitude for a decay and its CP-conjugate process have different magnitudes.
3. CP violation in the interference of decays with and without mixing, which occurs in decays into final states that are common to  $B^0$  and  $\bar{B}^0$ .

### 1.5.1 Cabbibo Kobayashi Maskawa (CKM) Matrix

At present the observed CP-violating effects arising in the neutral K-meson system can be incorporated successfully in the SM of electroweak interaction, within the framework of SM, CP violation is closely related to the quark mixing matrix, the CKM matrix connecting the electroweak eigenstates ( $d, s, b$ ) of the d, s and b-quarks with their mass eigenstates ( $d', s', b'$ ) through the following unitary transformation[2],

$$\begin{pmatrix} d' \\ s' \\ b' \end{pmatrix} = V_{CKM} \begin{pmatrix} d \\ s \\ b \end{pmatrix} \quad (1.5.1)$$

$$V_{CKM} = \begin{pmatrix} V_{ud} & V_{us} & V_{ub} \\ V_{cd} & V_{cs} & V_{cb} \\ V_{td} & V_{ts} & V_{tb} \end{pmatrix} \quad (1.5.2)$$

By definition the CKM matrix is a unitary matrix:

$$\hat{V}_{CKM}^\dagger \cdot \hat{V}_{CKM} = \hat{1} = \hat{V}_{CKM} \cdot \hat{V}_{CKM}^\dagger \quad (1.5.3)$$

Unitarity of CKM Matrix implies:

$$\sum_i V_{ij}^* \cdot V_{ik} = \begin{cases} 0 & \text{if } (j \neq k) \\ 1 & \text{if } (j = k) \end{cases} \quad (1.5.4)$$

where  $(i,j,k = 1,2,3)$

## 1.6 B Physics

### 1.6.1 Bottom Quark

In 1977, an experiment (CFS E288) led by physicist and Nobel laureate Leon Lederman at Fermilab provided the first evidence for the existence of the bottom quark [3]. The experiment discovered a particle, now called the upsilon ( $\Upsilon$ ), with a mass of 9.5GeV, composed of a new kind of quark (bottom) and its antimatter partner (anti-bottom). At the time of discovery, it was the most massive particle ever discovered. It has mass of 4.20 GeV[4], bottomness number -1, spin  $\frac{1}{2}$ , isospin 0 and even parity. The bottom quark can decay either into up or charm quark via weak interaction.

### 1.6.2 Production of $B_s^0$ Mesons at Hadron Colliders

A  $B_s^0$  meson consists of a anti b-quark and s-quark and is in pseudoscalar state. Its anti particle is made up of b-quark and anti s-quark. It has a mass of  $5.369\text{GeV}/c^2$ .

The present and the coming generations of hadron colliders provide an excellent laboratory to study the physics of b-flavoured hadrons. The large production cross sections and high luminosities, achievable in hadron colliders allows them to compete with  $e^+e^-$  machines, despite the low branching fraction of  $b\bar{b}$ -pairs production in hadron collisions (Table 1.3). In addition, the present  $e^+e^-$  colliders at SLAC and KEK work at center-of-mass energies of the  $\Upsilon(4S)(10.58\text{GeV})$  resonance, where some of heavy b-flavoured hadrons heavier than  $B^\pm$  or  $B_d^0$  (such as  $B_s^0$ ,  $\Lambda_b$ , etc) cannot be produced.

These facts make the hadron colliders by far the largest source of the b-flavoured hadrons. After the launch of the Large Hadron Collider (LHC) at CERN, scheduled for 2007, this pp machine with center-of-mass energy of 14 TeV, and luminosities ranging from  $10^{33}\text{cm}^{-2}\text{s}^{-1}$  to  $10^{34}\text{cm}^{-2}\text{s}^{-1}$  will become the worlds leading b-physics facility.

Table 1.3: The  $b\bar{b}$ -pair production at LHC and other accelerators.

	<b>B-factories</b>	<b>LEP</b>	<b>Tevatron</b>	<b>LHC</b>
<b>Prod. mode</b>	$e^+e^- \rightarrow \Upsilon(4S) \rightarrow b\bar{b}$	$e^+e^- \rightarrow Z^0 \rightarrow b\bar{b}$	$p\bar{p} \rightarrow b\bar{b} + X$	$pp \rightarrow b\bar{b} + X$
<b>CM energy</b>	10.58GeV	91.2GeV	1.8TeV	14TeV
$\sigma(b\bar{b})$	1.25nb	7.7 nb	$\sim 50 \mu\text{b}$	$\sim 500 \mu\text{b}$
$\sigma(b\bar{b})/\sigma_{tot}$	0.25	0.22	$\sim 6 \cdot 10^{-4}$	$\sim 2 \cdot 10^{-3}$

In hadron collisions, heavy quark pairs are produced in the strong interaction of

the partons composing the incoming hadrons. The cross section of this process can be estimated in QCD [5]. At the leading order the heavy quark pairs are mostly produced via gluon fusion (Fig. 1.1a), quark-antiquark annihilation  $q\bar{q} \rightarrow Q\bar{Q}$  (Fig. 1.1b) and gluon splitting processes  $g\bar{g} \rightarrow Q\bar{Q}$  (Fig. 1.1c). In case of high energy pp collisions, the latter two processes make dominant contributions to the total cross section. The inclusion of the next-to-leading order diagrams into the calculation of the cross section is discussed in [6] and the case of  $b\bar{b}$ -pair production at the LHC are studied in detail in [7] and [8]. The cross section is estimated to be approximately  $500\mu b$ , where the contributions from the gluon fusion, gluon splitting and flavour excitation processes are found to be of the comparable order in the calculation of the cross section and is very complicated, however the prospects.

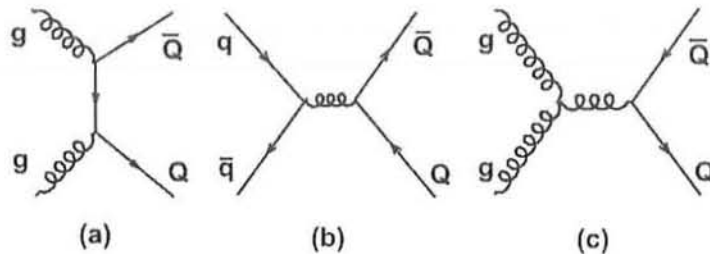


Figure 1.1: Some of the leading order diagrams, describing heavy-flavour production in hadron collisions.

After the  $b\bar{b}$ -pair is produced in hadron collision, the quark and antiquark undergo hadronization (fragmentation) into b-flavoured hadrons. The probability of the quark  $Q$  to fragment into a meson ( $Q\bar{q}$ ) is described by so-called *fragmentation functions*. The cross section of the production of the given b-flavoured meson in hadron collision

can be found by convoluting the QCD cross section with the corresponding fragmentation function. In the case of the CMS experiment at LHC, the value of  $\text{BR}(\bar{b} \rightarrow B_s^0) \simeq 0.107$  is suggested for the branching fraction of the  $\bar{b}$  quark fragmentation into the  $B_s^0$  meson [8].

### 1.6.3 The $B_s^0 \rightarrow J/\psi \phi \rightarrow \mu^+ \mu^- K^+ K^-$ Decay at CMS

In the  $B_s^0$  decay the strange quark serves as a spectator quark while the  $\bar{b}$  quark turns into  $\bar{c}$  quark with the emission of  $W^+$  Boson which further decays to  $c, \bar{s}$  quark. The  $c\bar{c}$  forms  $J/\psi$  while  $s\bar{s}$  forms  $\phi$  meson. The Feynman diagram for  $B_s^0 \rightarrow J/\psi \phi$  decay exhibiting the  $b(\bar{s}) \rightarrow c\bar{c}s(\bar{s})$  transition is shown in Fig. 1.2.

The  $B_s^0 \rightarrow J/\psi \phi$  decay channel followed by  $J/\psi \rightarrow \mu^+ \mu^-$  and  $\phi \rightarrow K^+ K^-$  decays, which is the aim of the current study, is a particular case of the  $B_s^0$  decay into the CP eigenstates. This channel is usually referred to as a gold-plated transition, because it allows the investigation of  $\Delta m_s, \Delta \Gamma_s, \bar{\Gamma}_s, \Gamma_s^H, \Gamma_s^L$ , as well as the extraction of the Wolfenstein parameter  $\eta$  [9], fixing the height of the unitarity triangle [10].



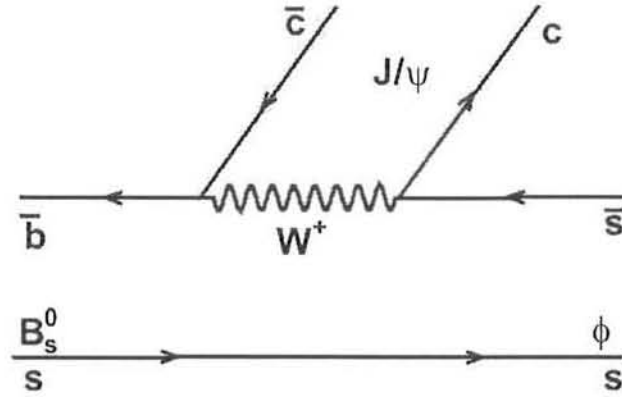


Figure 1.2: colour suppressed diagram for  $B_s^0 \rightarrow J/\psi\phi$

Some of the leading order diagrams, describing heavy-flavour production in hadron collisions.

The decay  $B_s^0 \rightarrow J/\psi\phi \rightarrow \mu^+\mu^-K^+K^-$  is of particular interest, since it allows the study many of properties of the  $B_s^0$  system, such as the differences between the widths and the masses of the two weak eigenstates,  $B_s^H$  and  $B_s^L$ . Contrary to the  $B^0$  system, the difference between the widths  $\Delta\Gamma_s$  of the two weak eigenstates is expected to be large, with a relative difference  $\Delta\Gamma_s/\bar{\Gamma}_s$  predicted to be of the order of 10% in the Standard Model. The first measurement from CDF ( $\Delta\Gamma_s/\Gamma_s = 65_{-33}^{+25}\pm 1\%$ ) [11] and the new preliminary result from DØ ( $\Delta\Gamma_s/\Gamma_s = 15\pm 10_{-4}^{+3}\%$ ) [12] have discrepancies between the two measured values themselves and with the Standard Model prediction. It is only very recently that a first measurement of the mass difference,  $\Delta m_s$  [13], has been performed at CDF. Time integrated measurements are not possible, as the time-integrated mixing probability saturates at a value of 0.5 for large mass differences,

and in time-dependent measurements, the high mass difference generates very rapid oscillations.

As in the  $B_s^0$  system the ratio  $\Delta m_s/\Delta\Gamma_s$  depends on the ratio  $|V_{cb}V_{cs}|/|V_{tb}V_{ts}|$ , which is quite well known, and on QCD corrections, a measurement of  $\Delta\Gamma_s$  would therefore yield an independent measurement of  $\Delta m_s$ . With the measurement already performed in the  $B^0$  system, the ratio between the mixing parameters of the  $B^0$  and  $B_s^0$  could provide a measurement of the ratio  $|V_{ts}|/|V_{td}|$ .

Furthermore this decay provides one of the best ways to determine the height of the Unitarity Triangle,  $\eta$  in the Wolfenstein parametrization. At first order of the Wolfenstein parameterization, the CP-violating weak phase  $\phi_{CKM} = [\arg(V_{cs} * V_{cb}) - \arg(V_{ts} * V_{tb})]$ , measured in the rate asymmetry cancels, and higher order terms have to be taken, yielding a weak phase  $\phi = 2\lambda^2\eta$ . The weak phase is therefore expected to be very small, of the order of 0.03. The measurement of a significantly large phase would indicate contributions from non-Standard Model processes.

The total  $b\bar{b}$  production cross-section at  $\sqrt{s} = 14$  TeV is expected to be as high as  $500\mu\text{b}$ . The cross section for the decay chain  $B_s^0 \rightarrow J/\psi \phi$  at LHC energies, including also the kinematic cuts also, can be given as follow[14]:

$$\sigma(B_s^0 \rightarrow J/\psi\phi) = \sigma(b\bar{b}).BR(\bar{b} \rightarrow B_s^0).BR(B_s^0 \rightarrow J/\psi\phi).BR(J/\psi \rightarrow \mu^+\mu^-).BR(\phi \rightarrow K^+K^-).\epsilon_{kine}$$

where the factor  $\epsilon_{kine} = (2.5890 \pm 0.0024)\%$ , which is the probability for the final decay products to pass the kinematical cuts, is obtained from the SIMUB Monte Carlo generator.

$$\text{where } \sigma(b\bar{b}) = 500\mu\text{b},$$

$$BR(\bar{b} \rightarrow B_s^0) = (10.7 \pm 1.1)\%,$$

$$BR(B_s^0 \rightarrow J/\psi\phi) = (9.3 \pm 3.3) \cdot 10^{-4},$$

$$BR(J/\psi \rightarrow \mu^+\mu^-) = (5.88 \pm 0.10)\%,$$

$$BR(\phi \rightarrow K^+K^-) = (49.1 \pm 0.6)\%,$$

$$\epsilon_{kine} = (2.5890 \pm 0.0024)\%$$

$$\sigma(B_s^0 \rightarrow J/\psi\phi \rightarrow \mu^+\mu^-K^+K^-) = (74 \pm 27) \text{pb}.$$

With kinematic requirements, using the world average branching ratios for the decays of  $B_s^0 \rightarrow J/\psi\phi \rightarrow \mu^+\mu^-K^+K^-$  the cross-section for our channel is predicted to be  $74 \pm 27 \text{ pb}$ . The number of  $B_s^0 \rightarrow J/\psi\phi \rightarrow \mu^+\mu^-K^+K^-$  events produced at CMS with different Integrated luminosities are shown in the Table 1.4.

Table 1.4: The number of  $B_s^0 \rightarrow J/\psi\phi \rightarrow \mu^+\mu^-K^+K^-$  Events produced per year at CMS.

	Low	Medium	High
Instantaneous Luminosity ( $\mathcal{L}$ ) $\text{cm}^{-2}\text{s}^{-1}$	$1 \times 10^{32}$	$1 \times 10^{33}$	$1 \times 10^{34}$
Integrated Luminosity for 1 year(L) $\text{nb}^{-1}$	$1 \times 10^6$	$1 \times 10^7$	$1 \times 10^8$
No of Events/year $N = L \cdot \sigma$	$7.4 \times 10^4$	$7.4 \times 10^5$	$7.4 \times 10^6$

A first measurement of one of the main parameters of the  $B_s^0$  system, the relative difference of the weak eigenstates, could be determined with a statistical uncertainty of 0.011 in a sample corresponding to an integrated luminosity of  $10 \text{ fb}^{-1}$ . A first measurement undertaken on approximately  $1.3 \text{ fb}^{-1}$  of data could already yield a measurement with an uncertainty of 20%. A natural extension of this study should be a tagged analysis, for which flavor tagging algorithms need to be developed.

### 1.6.4 Angular Analysis

The final state of the  $B_s^0 \rightarrow J/\psi\phi$  decay is an admixture of the CP eigenstates. Since  $J/\psi$  and  $\phi$  are massive vector mesons ( $J^{PC} = 1^{--}$ ) with the same (even) CP, their zero-angular-momentum spectrum consists of states with orbital angular momenta  $L = 0, 1, 2$  (even, odd and even respectively). The angular dependencies of CP-odd and CP-even components are different and can be separated through their angular distributions.

The angular distributions of the final state components can be described with only three physical angles. Typically the angular analysis is performed in the helicity frame shown in (Fig. 1.3). In the rest frame of the  $B_s^0$  the direction of flight of the  $\phi$  meson defines the  $z$ -axis. The  $x$ -axis is defined as arbitrary fixed direction in the plane normal to the  $z$ -axis. The  $y$ -axis is then fixed uniquely via  $y = z \times x$ . The right-handed coordinate system is assumed.

The angles  $(\Theta_{l^+}, \chi_{l^+})$  describe the direction of the  $\mu^+$  in the rest frame of the  $J/\psi$ . The angles  $(\Theta_{K^+}, \chi_{K^+})$  give the direction of  $K^+$  in the  $\phi$  rest frame. The third physical angle  $\chi$  is defined as  $\chi = \chi_{l^+} - \chi_{K^+}$  [10].

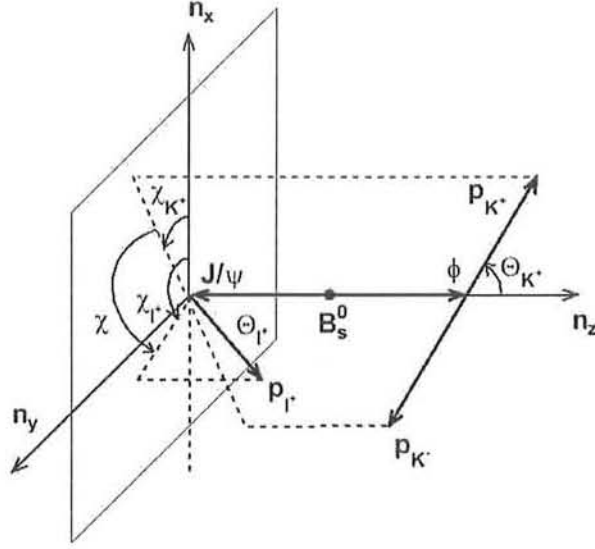


Figure 1.3: Definition of three angles  $\Theta_{l^+}$ ,  $\Theta_{l^-}$ ,  $\chi_{l^+}$ , describing the kinematics of the  $B_s^0 \rightarrow J/\psi\phi$  decay chain in the helicity frame of reference.

In general, the angular distributions of the final state components have the following form:

$$\frac{d^4\Gamma}{d \cos \Theta_{l^+} d \cos \Theta_{K^+} d\chi dt} \sim \sum_{i=1}^6 b_i(t) g_i(\Theta_{l^+}, \Theta_{K^+}, \chi), \quad (1.6.1)$$

where  $g_i(\Theta_{l^+}, \Theta_{K^+}, \chi)$  are the angular distributions, depending on the kinematics of the final state and  $b_i(t)$  are the time evolution of physical observables. The quantities  $b_i(t)$  are the bilinear combination of transversity amplitudes corresponding to the linear polarization of the final state  $A_0(t)$ ,  $A_{\parallel}(t)$  and  $A_{\perp}(t)$  [15].

The way of extracting the mixing parameters [8,9] and the CP violating Wolfenstein parameter  $\eta$  [9] in the  $B_s^0 \rightarrow J/\psi\phi \rightarrow \mu^+\mu^- K^+K^-$  decay is provided by the study of the angular distributions of the final state. One of the advantages of this

method is the possibility of extraction of the CKM phases. The method of angular analysis also provides a possibility to extract the frequency of particle-antiparticle oscillation from the flavour-tagged sample. This possibility is indeed attractive, since the  $B_s^0$  oscillations are very rapid and the possibility of their direct observation may be limited by the resolution of the detector.

The mixing in the  $B_s^0 - \bar{B}_s^0$  system gives rise to the mass eigenstates  $B_s^L$  and  $B_s^H$  with lifetimes which are expected to differ by about 10 to 30%. To a good approximation, CP violation can be neglected in calculating heavy and light mass eigenstates, in which case they correspond to the odd and even CP eigenstates respectively. The final state of the decay then represents an admixture of the CP-eigenstates.

## Chapter 2

# The CMS Experiment at LHC

The new frontiers of particle physics are the searches for extremely elusive particles, which are produced in processes with very low cross sections, the femto barn being the natural unit. With current technologies, leptonic colliders are not able to reach the high energies needed for these searches, which can presently be achieved only with hadron colliders. Despite the production of a lot of low energy particles resulting in a not clean environment, a proton-proton collider if compared to a leptonic interaction, offers the possibility to span over a wider energy spectrum that can be explored simultaneously and permits to reach higher production rates. These are the motivations for the CERN choice for the Large Hadron Collider (LHC).

## 2.1 The Large Hadron Collider at CERN

### 2.1.1 The Accelerator

The Large Hadron Collider LHC [16] will be the most powerful hadron collider expected to run next year. It is under construction in the already existing LEP [17] tunnel at CERN laboratories in Geneva, Switzerland. The Large Electron-Positron

collider LEP, which ceased to operate in the year 2000, was a circular  $e^+e^-$  accelerator, situated about 100m deep underground across the French-Swiss border. The new accelerator LHC will produce collisions between proton beams with centre of mass energy  $\sqrt{s}=14\text{TeV}$ , the highest value ever reached in accelerator experiments. It was planned to produce the first collision in April 2007 and start the physics program from August 2007, but unfortunately it would be somewhat late due to some technical problems. To reach such an energy, proton beams will be accelerated by existing CERN facilities of (Fig. 2.1), which will be upgraded. Protons will be accelerated and brought up to 50MeV by a linear accelerator LINAC. A Booster will raise the beam energy up to 1.4GeV injecting proton beams into the old circular accelerator PS (Proton Synchrotron). The 25GeV energy beams extracted from PS will be injected to a bigger circular accelerator SPS (Super Proton Synchrotron), which will introduce 450GeV proton beams into the LHC ring. The tunnel of LHC is a 26.659km circumference, composed of 8 curvilinear sections (2.840 km) and 8 rectilinear sections, where the beams are brought to collide. The accelerating power of LHC is limited by the bending magnetic field needed to keep the beams circulating in the tunnel, and is

$$p[\text{GeV}/c] = 0.3B[\text{T}]\rho[\text{m}] \quad (2.1.1)$$

where B is the magnetic field supplied to maintain particles with momentum  $p$  in a circular orbit with radius  $\rho$ . The choice of 7TeV beam energy is forced by the maximum achievable magnetic fields and depends on the radius (4.3km) of the existing tunnel, resulting in Magnetic field (5.4T) (Table 2.1). For the collisions which occur between particles of the same kind, a unique magnetic field is required to accelerate the proton beams in opposite directions and the two beam pipes will be inserted into



a single cryostatic structure with the superconducting magnets and the corresponding coils.

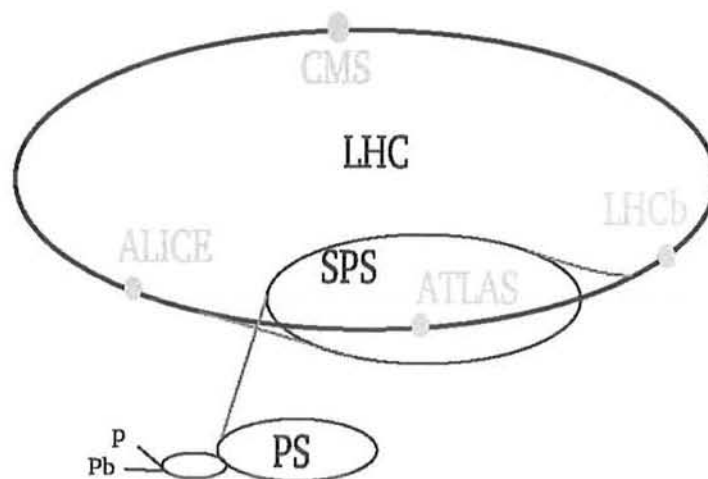


Figure 2.1: Overview of LHC with four main detectors.

After its launch, scheduled for year 2008, LHC will become the world leading facility for high-energy hadron physics. Since two beams with particles of equal charge are to collide in LHC, dipole magnetic fields of opposite polarity are required for both beams. The LHC beams are therefore separated, each having its own acceleration ring, superconducting dipole magnets and vacuum chambers. The beams share only the short fractions of the beam pipe in the experimental areas.

The event rate at the LHC can be estimated using the relation.

$$R = L\sigma \quad (2.1.2)$$

Where  $\sigma$  is the cross section of the events under study. The proportionality factor  $L$  in (Eq.2.1.2), called luminosity, represents the technical characteristics of the collider, depending on the beam parameters such as number of particles per bunch, revolution frequency, transverse beam profiles, beam-to-beam crossing angles and others.

In pp collisions at LHC, the maximal luminosity of  $2 \times 10^{33} \text{cm}^{-2} \text{s}^{-1}$  during the phase-I (first several years of operation) and of  $10^{34} \text{cm}^{-2} \text{s}^{-1}$  during the phase-II of the accelerator is intended to be achieved [18]. The main technical properties of the LHC accelerator, when working at peak luminosity in pp collision mode, are summarized in (Table 2.1).

At present, there are four experiments (Fig. 2.1), in preparation for working at the LHC environment in the proton-proton collisions mode. Two of them, CMS [19] and ATLAS [20], are the general-purpose detectors, designed to work at the peak luminosities mentioned above. The main goals of these two collaborations is the exploration of the limits of the Standard Model, searches of Standard Model and Supersymmetric Higgs bosons, supersymmetric partners of the Standard Model particles and high precision physics of t and b quarks.

The other two experiments, scheduled to work in proton-proton collision mode are LHCb [21] and ALICE [22]. The LHCb experiment is dedicated for the b-physics studies at the luminosity of  $10^{32} \text{cm}^{-2} \text{s}^{-1}$ . The LHC accelerator will also run with collisions between beams of lead ( ${}_{208}\text{Pb}^{82+}$ ) ion. The heavy ion collisions will be principally studied at specialized ALICE experiment, with CMS and ATLAS also having a heavy ion programs.

Table 2.1: Technical properties of the Large Hadron Collider at CERN, relevant to the pp high luminosity mode.

Circumference	26.659 km
Maximum Dipole field	8.33 T
Magnet Temperature	1.9 K
Beam energy at injection	450 GeV
Beam energy at collision	7 TeV
Nominal Luminosity	$1 \times 10^{34} \text{ cm}^{-2} \text{ s}^{-1}$
Number of Bunches	2808
Number of particles per bunch	$1.15 \times 10^{11}$
Bunch separation	24.95 ns
Total crossing angle	285 $\mu\text{rad}$
Bunch Length (r.m.s.)	7.55 cm
Transverse beam size at Impact Point	15 $\mu\text{m} \times 15 \mu\text{m}$
Luminosity lifetime	13.9 h
Filling time per ring	4.3 min
Energy loss per turn	7 keV
Total radiated power per beam	3.8 kW
Stored energy per beam	362 MJ

### 2.1.2 Main Goals of LHC

Our current understanding of the universe is incomplete. The Theories that we currently use to describe it leave many unsolved questions.

- The reason why elementary particles have mass and why their masses are different are among the most perplexing questions. The answer may be the so-called Higgs mechanism. The Higgs field has at least one new particle associated with it, the Higgs boson. If such a particle exists, the LHC will be able to detect it.
- A very popular idea that could partly explain why all the matter we see in the Universe counts for only 4% of the total mass, is called supersymmetry, or SUSY. SUSY predicts that for each known particle there is a 'supersymmetric' partner. If SUSY is right, then supersymmetric particles should be found at the LHC.
- The LHC will also help us to solve the mystery of antimatter. Matter and antimatter must have been produced in the same amounts at the time of the Big Bang. From what we have observed so far, our Universe is made of only matter. Why The LHC could provide an answer.

## 2.2 The CMS Detector

The Compact Muon Solenoid (CMS) [23] is a multipurpose particle detector designed to study proton-proton collisions at the Large Hadron Collider at CERN (Fig. 2.2).

### 2.2.1 General layout of CMS

The Compact Muon Solenoid experiment, CMS [24], is a general purpose detector which will operate at LHC. The main feature of CMS is the 4 T superconducting solenoid that permits a compact design of the detector with a strong magnetic field. The design priorities fulfilled by the CMS project [25] are a redundant muon system, a good electromagnetic calorimeter and a high quality tracking system.

The structure of CMS is typical of a general purpose experiment designed for a collider: several cylindrical layers coaxial to the beam direction, referred to as barrel layers, closed at both ends by detector disks orthogonal to the beam pipe, the endcaps, to ensure detector hermeticity. In Fig. 2.2 a schematic view of CMS is drawn pointing out the cylindrical symmetry of the experiment, which has a full length of 21.6m, a diameter of 15m and reaches a total weight of 12500 ton.

The natural coordinate frame used to describe the detector geometry is a right-handed Cartesian system with the x-axis pointing to the centre of the LHC ring, the z-axis coincident with the CMS cylinder axis and the y-axis directed almost upwards along the vertical. The cylindrical symmetry of CMS design and the invariant description of pp physics drive to use a pseudo-angular reference frame, given by the triplet  $(r, \phi, \eta)$ , with r being the distance from z axis,  $\phi$  azimuthal coordinate with respect to x axis and pseudorapidity( $\eta$ ). In this reference frame it is easy to describe the CMS subdetectors, that are installed radially from inside out.

The CMS detector has two main parts as follows:

1. The Barrel Region
2. The Endcap Region

- (a) Forward Region
- (b) Backward Region
- (c) The Very Forward Calorimeter

The CMS subdetectors and magnet, that are installed radially from inside out are:

- **Tracker:**  $r < 1.2\text{m}$  ,  $|\eta| < 2.5$  Silicon pixel vertex detector plus  $198\text{m}^2$  active area of Silicon microstrip detectors to reconstruct charged particle tracks and identify primary and secondary vertices.
- **ECAL:**  $1.2\text{m} < r < 1.8\text{m}$  ,  $|\eta| < 3$  electromagnetic calorimeter to precisely measure electrons and photons, composed by  $\text{PbWO}_4$  scintillating crystals and a forward preshower detector.
- **HCAL:**  $1.8\text{m} < r < 2.9\text{m}$  ,  $|\eta| < 5$  hadron calorimeter system for jet position and transverse energy measurements, extended in the forward region  $3 < |\eta| < 5$  with a very forward calorimeter (HF).
- **Magnet:** Coil  $2.9\text{m} < r < 3.8\text{m}$  ,  $|\eta| < 1.5$  the magnet, large enough to accommodate most of the calorimeters and the inner tracker, with a 4T longitudinal magnetic field supplied by a superconducting solenoid.
- **Muon System:**  $4.0\text{m} < r < 7.4\text{m}$  ,  $|\eta| < 2.4$  muon chambers merged inside the magnet yoke to detect and reconstruct muon tracks, composed by Drift Tubes (DT) in the barrel and Cathode Strip Chambers (CSC) in the endcaps and complemented overall up to  $|\eta| < 2.1$  by Resistive Plate Chambers (RPC).

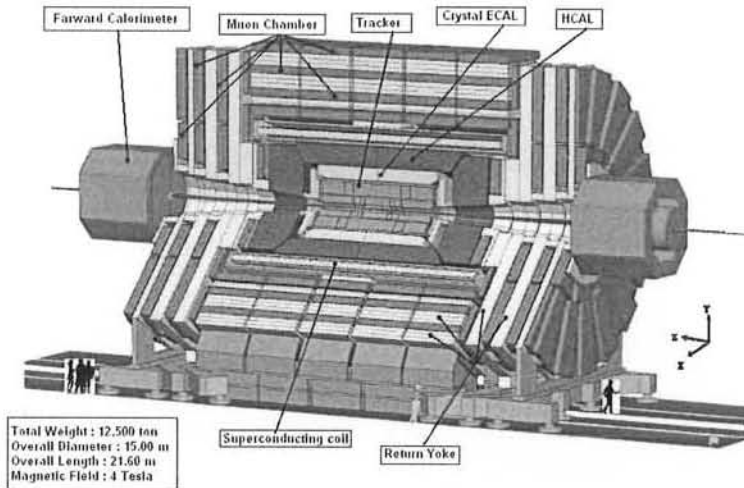


Figure 2.2: General layout of the CMS detector at the Large Hadron Collider at CERN.

## 2.3 Geometry of CMS

### 2.3.1 The Magnet

The CMS magnet [26] is a 13 m long superconducting solenoid with a diameter of 5.9m. It provides an inner uniform 4T magnetic field, to permit precise measurements of charged particle transverse momentum with a large bending power.

The conductor consists of three concentric parts: a central superconducting cable, a high purity aluminium stabilizer and an external aluminium alloy to reinforce the sheath. The superconducting cable is a Rutherford type with 40 NiTb strands and is kept cooled by a liquid helium cryogenic system. The magnetic flux is closed in a

loop via a 1.8 m thick saturated iron yoke, instrumented with four muon stations.

The coil accommodates the tracking system and most of the calorimeters and it is also a supporting structure for the inner part of the apparatus, because it is the main element in terms of size, weight and mostly structural rigidity.

### 2.3.2 The Tracker

The silicon tracker [27] is inner detector of CMS. It is the closest to the interaction point and represents an essential detector to address the multiplicity of LHC physics goals. It extends in the region  $|\eta| < 2.5$ ,  $r < 120\text{cm}$ ,  $|z| < 270\text{cm}$  and it is completely based on semiconductor detectors made of silicon covering the largest ever-designed Si detector surface of  $198\text{ m}^2$ . Using the tracker, vertices and charged particle tracks have to be reconstructed in the highly congested LHC environment. To better solve the pattern recognition problem, the tracker is designed to fulfill two basic properties: low cell occupancy and large hit redundancy. For these reasons it is structured in an inner silicon pixel detector surrounded by several layers of silicon microstrip detectors of different size and pitch between the strips. The low occupancy is obtained by working with high granularity detectors, mainly the ones closer to the interaction point because they have to cope with higher particle fluxes, and fast primary charge collection, obtained with thin detectors and overdepleting the silicon bulks. Redundancy is guaranteed by the overall design, which allows many measured points per track within an acceptable material budget to avoid impairing the electromagnetic calorimeter performance too much. In this way an average of 12-14 points (hits) per track are guaranteed to permit a high tracking efficiency and a low rate (10.3 or less) of fake tracks, which are reconstructed tracks but do not corresponding to any real track. A



consequence of high particle density is the radiation damage of the silicon sensors.

### 2.3.3 The Electromagnetic Calorimeter (ECAL)

A high performance Electromagnetic Calorimeter (ECAL) is a fundamental requirement for any general purpose LHC experiment for precise measurements of electrons and photons. The design of CMS ECAL [28] has been prompted by the possibility of observing the decay of a light Higgs boson into a pair of photons. Since in the region  $m_H < 140 \text{ GeV}/c^2$  the intrinsic Higgs width  $\Gamma_H$  is less than 100 MeV, the invariant mass resolution is dominated by experimental resolution, which should be of the order of 1% to enhance the significance of a possible signal.

The CMS collaboration has chosen a homogeneous calorimeter composed of finely segmented crystals of lead tungstate ( $\text{PbWO}_4$ ), which is a radiation resistant and chemically inert scintillator suited to work in the LHC high dose environment (from 0.18 Gy/h at  $|\eta| = 0$  to 6.5 Gy/h at  $|\eta| = 2.6$  at high luminosity). Moreover, lead tungstate also has a short scintillation decay time = 10 ns that allows to collect 85% of the light in the 25 ns interval between two pp collisions. The small Moliere radius  $r_7$  of 21.9 mm and radiation length 8.9 mm permit the shower containment in a limited space resulting in a compact calorimeter design. It is organized in a barrel region  $|\eta| < 1.48$  and a forward region to cover the pseudorapidity area below 3.0. It is composed of 61,200 crystals in the barrel region and 21,528 in the endcaps grouped in 36 supermodules. The crystals have trapezoidal shape with squared front faces and are slightly different in the two regions: in the barrel they are 230 mm long with a total radiation length  $25.8 X_0$  and  $22 \times 22 \text{ mm}^2$  front section, equal to the Moliere radius. The granularity is  $\Delta\eta \times \Delta\varphi = 0.0175 \times 0.0175$ , high enough for efficient  $\pi^0 - \gamma$

separation. The collection of light is performed with silicon avalanche photodiodes (APD), which are able to operate inside a high magnetic field and can address the low light-yield of the crystals.

In the endcaps, the crystals have  $24.7 \times 24.7 \text{ mm}^2$  square front sections and smaller length (220 mm) and hence a smaller radiation length ( $24.7X_0$ ), because in front of the endcaps a preshower with  $X = 3X_0$  in the two regions  $1.65 < |\eta| < 2.6$  is foreseen. Each preshower is composed of two lead radiators and two planes of silicon microstrips to increase the  $\pi^0$  rejection power in the highly irradiated forward regions, which are also affected by the decrease in performance due to the larger granularity at higher  $|\eta|$ , with a maximum value of  $\Delta\eta \times \Delta\varphi = 0.05 \times 0.05$  in the very forward crystals. The higher irradiation levels would also induce too high leakage currents in APDs, therefore the forward crystals are read by vacuum photo-triodes (VPT).

### 2.3.4 The Hadron Calorimeter

The Hadron Calorimeter (HCAL) is used together with the electromagnetic one to measure the energy and direction of jets, the transverse energy  $E_T$  and the imbalance of transverse energy, or missing transverse energy,  $E_T^{miss}$ . To fulfill these requirements, it has to be thick enough to contain the whole hadron shower and have high hermeticity. Since it is placed inside the magnet, it can not be made with ferromagnetic materials. The CMS HCAL [29] is a sampling calorimeter with 3.7mm thick active layers of plastic scintillators alternated with 5cm thick brass plate absorbers. The signal is readout with wavelength-shift fibres. The granularity  $\Delta\eta \times \Delta\varphi = 0.087 \times 0.087$  is fine enough to allow an efficient di-jet separation. It is subdivided, as can be seen in Fig. 2.22, into barrel ( $|\eta| < 1.4$ ) and endcap ( $1.4 < |\eta| < 3.0$ ) with an overall thickness

varying from 8.9 to 10 interaction lengths  $\lambda_0$  respectively.

Since the barrel part of the calorimeter is not sufficiently thick to contain all the energy of highly energetic showers, an additional “tail-catcher” of scintillator tiles is located outside the magnet. To improve the pseudorapidity coverage from  $|\eta| = 3$  to  $|\eta| = 5$ , a very forward calorimeter (HF) is placed outside the magnet yoke, 11 m away along the beam direction from the nominal interaction point. It is another sampling calorimeter with active elements made of quartz fibres parallel to the beam interleaved into steel plate absorbers. The active elements, whose granularity is  $\Delta\eta \times \Delta\varphi = 0.17 \times 0.1745$ , are sensitive to Cherenkov light and are readout with photomultiplier tubes. With this configuration the complex of CMS hadron calorimeters has an overall depth of more than  $11\lambda_0$  over the full  $|\eta| < 5$  coverage.

### 2.3.5 The Muon System

The muon system [30] is placed outside the magnet, embedded in the iron return yoke to make full use of the 1.8T magnetic return flux. It plays an essential role in the CMS trigger system, because high  $p_T$  muons are clear signatures of many physics processes. The main goal of this system is to identify muons, and when combined with the tracker, measure their transverse momentum  $p_T$ , and it is also used for precise time measurement of the bunch crossing [31].

It is organized into three independent subsystems shown in the barrel, where the track occupancy is relatively low ( $< 10$  Hz/cm<sup>2</sup>), and drift tubes (DT) are installed, while in the endcaps cathode strip chambers (CSC) are favoured to work with higher particle rates ( $> 100$  Hz/cm<sup>2</sup>) and a larger residual magnetic field within the yoke plates. These two subsystems cover the  $|\eta| < 2.4$  region and are arranged in a

multi-layer structure to efficiently reject single hits produced by low range particles. In the region  $|\eta| < 2.1$  redundancy is provided by resistive plate chambers (RPC), which have a limited spatial resolution, but a faster response and excellent time resolution, less than 3ns. They are used mainly for unambiguous bunch crossing identification and also to complement the DT+CSC measurement of  $p_T$  during the trigger period, because RPCs can be finely segmented since they do not demand a costly readout system. Drift Tubes are composed of parallel aluminium plates insulated from perpendicular “I” shaped aluminium cathodes by polycarbonate plastic profile. The anodes are 50mm diameter stainless steel wires placed between the “I” cathodes. The internal volume is filled with a binary mixture of 80% Ar and 20% CO<sub>2</sub> at atmospheric pressure, because this gas is non-flammable and can be safely used in underground operations in large volumes, as required in CMS. Each of the drift tube stations is composed of three groups (superlayers) of four layers of drift tubes, of which two are parallel to the beam axis for  $r$ - $\varphi$  measurement, while one is orthogonal for  $z$  measurement. The resolution is about 100mm both in  $r$ - $\varphi$  and  $r$ - $z$  views.

Cathode Strip Chambers are composed of arrays of anode wires between a pair of cathode planes, segmented into strips perpendicular to the wires. Gaps are filled with a gas mixture of 30% Ar, 50% CO<sub>2</sub> and 20% CF<sub>4</sub>. The interpolation of the signal of neighbouring strips allows a precise spatial measurement of the  $\varphi$  coordinate with 50mm resolution. Resistive Plate Chambers are made of planes of a phenolic resin (bakelite) with a bulk resistivity of  $10^{10}$ – $10^{11}$   $\Omega$ cm, separated from aluminium strips by an insulating film. The gaps are filled with a non-flammable gas mixture of 94.5% freon (C<sub>2</sub>H<sub>2</sub>F<sub>4</sub>) and 4.5% isobutane (i-C<sub>4</sub>H<sub>10</sub>), which operates in avalanche mode to

sustain the high rates.

### 2.3.6 The Trigger system

While pp collisions occur at a rate of 40 MHz, it is impossible to store on tape all the information about every collision, practical and technical difficulties impose a limit of about 100 Hz in the acceptable rate of permanently stored data. Furthermore, the rate of interesting events is smaller by order of magnitudes than the total interaction rate, hence a trigger system is built up with the two fold task to reject a factor  $4 \times 10^5$  of the collisions and to select in a short time the interesting physics events with high efficiency.

The CMS has two-step trigger and data acquisition system, designed to inspect the detector output at full bunch crossing frequency and to store the selected events at the maximal allowed storage rate of 100 Hz. The first level trigger (L1) is a hardware trigger designed to reduce the rate of accepted events to less than 100KHz. It is based on the identification of muons, electrons, photons, jets and missing transverse energy. The second level trigger or HLT (High Level Trigger) is a software trigger, running on the dedicated farm of commercial processors and designed to reduce the maximum L1 output rate to the final output rate of 100Hz. The bandwidth of 100Hz should then be shared between all the channels of interest.

#### Level-1 Trigger

The Level-1 trigger selection is based exclusively on calorimeter and muon chamber information, processed with hardware logical circuits [32], though with coarse granularity. The Level-1 trigger system is required to be capable of processing every 40MHz

pp collision and reduce to 100 kHz the data rate to pass to the HLT. At LHC startup the CMS Level-1 output rate will be reduced to only 50kHz for low luminosity and it will be raised to the designed 100kHz at full LHC luminosity.

### High-Level Trigger

The High-Level trigger [33] selection (HLT) is realized with a software running on a farm of commercial processors. The goal of HLT is to reduce the Level-1 output rate to 100Hz mass storage with dedicated ‘fast’ algorithms.

### 2.3.7 CMS Physics Motivation

The search for new particles and physics processes beyond the so-called Standard Model of particle physics is the main motivation of the CMS scientific program. The overall design of the detector is motivated by the variety of the physics signatures foreseen:

1. The major goal of CMS is the search for Standard Model and discovery of Higgs boson in proton-proton collisions at high luminosity, which is responsible for particle masses and the key element of the Standard Model. The Supersymmetric Higgs bosons can be searched at CMS.
2. The other important topic to study with CMS is the search for the supersymmetric partners of the Standard Model particles. If Supersymmetry is indeed realized in our world, CMS might be able to detect the decays of squarks and gluinos. To achieve this goal, final states with numerous jets and hard leptons should be studied.

3. Taking the advantage of working at the low luminosity ( $\mathcal{L} = 2 \times 10^{33} \text{cm}^{-2}\text{s}^{-1}$ ) mode during the first several years of the LHC operation, the CMS collaboration plans a number of studies in the field of b-physics. Here the most important topics are the study of the oscillation of the neutral b-flavoured mesons, study of the CP violation in B-decays, measurement of the parameters of the unitarity triangle. In addition to the  $B_s^0 \rightarrow J/\psi(\rightarrow l^+l^-) \phi(\rightarrow K^+K^-)$  channel, discussed in this thesis, decays  $B_d^0 \rightarrow J/\psi(\rightarrow l^+l^-) K_s(\rightarrow \pi^+\pi^-)$ ,  $B_d^0 \rightarrow \pi^+\pi^-$  (both for extraction of angle  $\beta$  of the unitarity triangle) and others will also be studied.
4. Also LHC environment provides an excellent laboratory to study the physics of the top quark. Even in the low luminosity phase of the accelerator,  $t\bar{t}$  pairs will be produced with a rate of about one per minute. The top quark was discovered at Tevatron in 1994 [34, 35], nevertheless its mass is still known with a relatively large uncertainty. The precise measurement of the top mass therefore becomes therefore one of the major goals of LHC.

In order to be able to detect efficiently the variety of physics signatures listed above, the design of the CMS detector should allow precise measurements of the photons, muons and electrons over a large energy range. Special care should be taken for the efficient detection of the soft muons coming from the b-decays. The detector should also provide a possibility for precise reconstruction of charged tracks over a large range of transverse momenta. Accounting for large multiplicity of charged particles in the hadron collisions and high luminosity of the LHC, the detector should be granular enough in order to minimize the probability of the pile up particles to be in the same detector unit as interesting object. In addition, the identification

of the b-decays, which is equally important for Higgs, t and b-physics, requires the reconstruction of secondary vertices with a very high space resolution.



# Chapter 3

## Software Package

### 3.1 Introduction

Many experiments in Nuclear Physics and Particle Physics need physics event generators. These will be used to drive the simulation and experimental proposals and test the analysis. In fact the validity of the finally results of some of the most complex experiments depends upon the quality of the event generator and the simulations.

An “**EventGenerator**” [36] is a piece of code which generates a list of events. Each event is a list of particles simultaneously seen in a detector. Typically each particle is parameterized by a particle-type, and an initial momentum vector. In addition an initial position or vertex may also be needed. “**Physics Event Generators**” produce events which are distributed to reflect an aspect of physics. Typically this means that the events are distributed throughout a detector in the same way as nature would distribute them.

Monte Carlo (MC) methods are a type of numerical calculation. They can be described as statistical simulations utilizing sequences of random numbers to perform

the simulation. MC techniques are used extensively in high energy physics experiments, where experimental data describing the physics of the interactions and their expected behavior in the detector are modeled and studied. Some of event generators are Pythia [37], QQ [38], and EvtGen [39].

SIMUB [40] is a Monte Carlo Event Generator of B-meson production and decays which is developed at Dubna for the Compact Muon Solenoid (CMS) Project at CERN. The main motivation for this activity was that, already existing generators do not take into account the theoretical refinements which are of great importance for MC studies of B-decay dynamics. In particular, in the generators PYTHIA , QQ, and EvtGen, the time-dependent spin angular correlations between the final-state particles are not included in the proper way for the so called “golden decay”  $B_s^0(t), \bar{B}_s^0(t) \longrightarrow J/\psi(\longrightarrow l^+l^-)\phi(\longrightarrow K^+K^-)$ .

The events are produced with the dedicated SIMUB generator, which uses PYTHIA for production and fragmentation of the  $b\bar{b}$  pairs. The dynamics of this decay is described by a four dimension probability distribution function depending on decay time and three physical angles. The algorithms of multidimensional random number generation have been elaborated and then implemented in the package SIMUB to provide tools for MC simulation of sequential two-body decays  $B^0(t), \bar{B}^0(t) \longrightarrow a(\longrightarrow a_1a_2)b(\longrightarrow b_1b_2)$  in accordance with theoretical time dependent angular distributions.

The study of decays  $B_s^0(t), \bar{B}_s^0(t) \longrightarrow J/\psi(\longrightarrow l^+l^-)\phi(\longrightarrow K^+K^-)$  , which is one of the gold plated channels for B-Physics studies at the LHC, looks very interesting from the physics point of view. It presents several advantages related to the dynamics of these decays, characterized by proper-time-dependent angular distributions of transversity amplitudes.

## 3.2 General structure of program SIMUB

The package for generation of production of B-mesons and their decays, SIMUB, is kept under the directory SIMUB which has the following main parts:

- `bb_gen` - routines needed to generate  $b\bar{b}$  events (FORTRAN, PYTHIA, HBOOK).
- `bb_frg` - routines performing string fragmentation and generation of B-mesons (FORTRAN, PYTHIA, HBOOK). The program is a part of `BB_dec` program but may be used as independent program.
- `BB_dec` routines performing B-decays (C++, FORTRAN, PYTHIA, HBOOK, ROOT) and storing the results into standard HEPEVT format Ntuple for further usage in the CMS detector simulation or in format JETSET for analysis (Fig. 3.1).

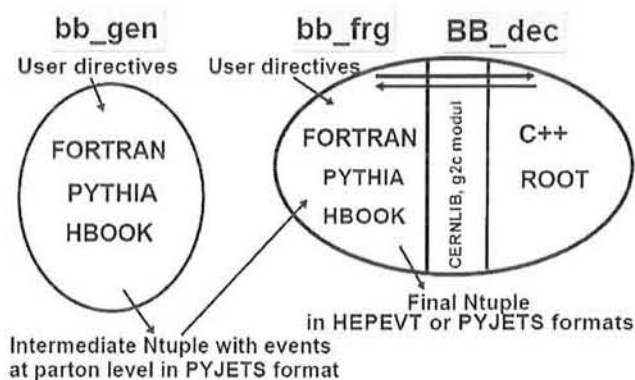


Figure 3.1: The flow of data within the package SIMUB.

- `include` - a collection of common blocks for `bb_gen`, `bb_frg` and `BB_dec`.

To simulate the B-meson production in pp collisions with PYTHIA (programs `bb_gen` and `bb_frg`), we used the modified routines from the FORTRAN-based package. The data flow between three main parts (`bb_gen`, `bb_frg`, and `BB_dec`) of the package SIMUB is organized in the following two steps:

- In the first step the  $b\bar{b}$ -events are generated by the program `bb_gen` and written to Ntuple `bb_X_YYY`.
- In the next step the program `BB_dec` reads  $b\bar{b}$ -events from Ntuple `bb_X_YYY` and performs the string fragmentation (via call `bb_frg`) and decay of B mesons. The decay modes and mechanisms are defined by user. The full information about B decay events is stored in Ntuple `BB_dec.ntpl`.

### 3.3 Event Generation

#### 3.3.1 Generation of $b\bar{b}$ in `bb_gen`

The “`bb_gen`” is the subdirectory of SIMUB package used to produce  $b\bar{b}$  events by using PYTHIA which further hadronize to  $B_s^0$  meson in further processes. In this subdirectory  $b\bar{b}$  events are produced and written to Ntuple “`bb_X_YYY`” as well as listing of the program which are stored in subdirectory `data BB/bb_gen_out`. That Ntuple further used in `bb_frg` as an input to generate the  $B_s^0$  meson. It contains some subdirectories as follows:

- `mak` – Makefile needed to create the executable and `example.run` script provided to run compiled program. In `bb_gen` run file following PYTHIA parameters are used to generate  $b\bar{b}$  events:

- set variable “bb\_gen\_out” - output directory.
  - NRUN is to define the run number (0...999).
  - NEVT sets the number of events to be produced.
  - MRPY sets the initial PYTHIA random number seeds (0...900000000); to obtain new events you need to change MRPY.
  - MSEL = 5 is used to produce  $b\bar{b}$  in every event.
- bin – preprocessed FORTRAN source files, compiled objects and executables.
  - ana – ROOT/C++ scripts provided for analysis.
  - src – The name of each source file in “bb\_gen/src” corresponds to the name of routine. All routines needed to generate  $b\bar{b}$  events are listed below:
    - “gen\_main.F” : Generates PYTHIA parton events containing  $b\bar{b}$  pairs, .
    - “gen\_uinit.F” : Reads user directives needed for program running and performs PYTHIA initialisation.
    - “gen\_hinit.F” : Defines and initialises outgoing Ntuple as well as some control histograms.
    - “gen\_loop.F” : Generates PYTHIA events within a loop.
    - “gen\_checkbb.F” : Checks if the event has b quark(s).
    - “gen\_hfill.F” : Fills the control histograms.
    - “gen\_write.F” : Stores the event information in outgoing Ntuple.
    - gen\_calc.F : Checks the subprocess type and counts the number of events for different types of  $b\bar{b}$ -production subprocesses.

- gen\_pylist.F : Provides the PYTHIA listing for each type of  $b\bar{b}$ -production subprocess.
- gen\_end.F : Termination routine. Adds the record with information about the run to the Ntuple.

To run  $b\bar{b}$  generation jobs, the user should go to the "bb\_gen/mak" directory. To compile sources, the "Makefile" is provided. It is enough to type "gmake", then execute it with command 'run' which creates Ntuple, for example bb\_5\_355, in which 5 and 355 shows MSEL and NRUN respectively.

### 3.3.2 b-quark Fragmentation into $B_s^0$ in bb\_frg

The files needed to perform string fragmentation and decays by PYTHIA are kept under the "bb\_frg" directory. In this program "bb\_frg" reads  $b\bar{b}$  events from the Ntuple "bb\_X\_YYY" and perform the string fragmentation and decays. The events are written down in Ntuple and listings are stored in subdirectory "dataBB/bb\_gen\_out/bb\_frg\_out". It contains subdirectories ana, mak, bin, src. The name of each source file in "bb\_frg/src" corresponds to the name of routine. These routines and directories are listed below :

- "frg\_main.F" : Main program to read generated  $b\bar{b}$  events from Ntuple "bb\_X\_YYY", perform string fragmentation and user dependent event processing by PYTHIA; placed in "bb\_frg/mak" directory.
- frg\_uinit.F : Reads user directives needed to run the program.
- frg\_pinit.F : Initialises PYTHIA.

- `frg_loop.F` : Within a loop over the required input files it opens input Ntuple, reads it event by event, closes input Ntuple, and finally, for each input file prints some statistical information.
- `frg_procevent.F` : the string fragmentation is performed with channels and selection which were set by user in "bb\_frg/mak/run" file.
- `gen_end.F` : Termination routine.

To build the fragmentation job, one has to go to his "SIMUB/bb\_frg/mak" directory. The compilation is similar to that for "bb\_gen" program.

### 3.3.3 $B_s^0$ decay and Analysis in BB\_dec

All "bb\_frg" functions can be done in program "BB\_dec". Additionally program "BB\_dec" can perform decays with complicated physics mechanism (with additional option "COPT SI1"). In this case program "BB\_dec" by calling "bb\_frg" routines reads  $b\bar{b}$ -events from Ntuple "bb\_X\_YYY" and performs the string fragmentation (PYTHIA) and decays (PYTHIA) apart of the  $B_s^0$ -meson decays, if the option with decay channel "COPT SI1" is set. In case "COPT SI1" the information about  $B_s^0$ -mesons (which will be decayed by physics mechanism) is written in PYJETS (PYTHIA) common block. Then program reads momentum and verteces of these B-mesons and performs  $B_s^0$ -decays. Information about decay products is written in PYJETS. Then "bb\_frg" stores all final particles in external files in directory "dataBB/bb\_gen\_out/BB\_dec\_out".

For compilation and Running of the BB\_dec Program and build the  $B_s^0$ -decay simulation, one has to go to "SIMUB/BB\_dec/mak" directory. The "Makefile" script may be found there. The user can not excute simply the command "gmake" because the

source files are placed in complicated tree of directories. There is a file `make_release` for this purpose. The main program is placed in “SIMUB/BB\_dec/mak” directory. To compile and run the program, one should go to “SIMUB/BB\_dec/mak” directory and execute the command `make_release`.

SIMUB includes following Decays of  $B_s^0$  and  $\bar{B}_s^0$  mesons:

- $B_s^0, \bar{B}_s^0 \rightarrow J/\psi(\rightarrow \mu^+ \mu^-) \phi(\rightarrow K^+ K^-)$ ,
- $B_s^0, \bar{B}_s^0 \rightarrow J/\psi(\rightarrow \mu^+ \mu^-) K^*(\rightarrow K^+ \pi)$ ,
- $B_s^0, \bar{B}_s^0 \rightarrow D_{-s}(\rightarrow K K) \mu \nu_\mu$

### 3.3.4 BtoVVana

The package BtoVVana [41] has been developed to analyze the decays of neutral pseudoscalar B-mesons into two vector mesons decaying into two muons and two pseudoscalar mesons. Two channels of this type are included in the B-physics generator SIMUB used here for precise testing of the package BtoVVana:

- $B_s^0, \bar{B}_s^0 \rightarrow J/\psi(\rightarrow \mu^+ \mu^-) \phi(\rightarrow K^+ K^-)$
- $B_s^0, \bar{B}_s^0 \rightarrow J/\psi(\rightarrow \mu^+ \mu^-) K^*(\rightarrow K^+ \pi)$

These channels contain rich physics information because of nontrivial angular distributions and time dependence of the decays. The package BtoVVana and program codes for the channels  $B_s^0 \rightarrow J/\psi \phi$  and  $B_d^0 \rightarrow J/\psi K^*$  in the Monte Carlo generator SIMUB were written in parallel and mutually tested with high precision. The systematic study of these decays will be performed after year 2007 on the LHC detectors. About 200,000  $B_s^0 \rightarrow J/\psi \phi$  events at the CMS, 100000 events at the ATLAS



and 75 000 events at the LHCb are expected to be available during first year of low luminosity operation.

Files of the package BtoVVana are kept under the BtoVVana directory which contains subdirectories mak, src, doc, res.

- src contains the source codes of the program.
- mak contains Makefile, command files for compilation make release and execution run.
- bin contains the results of the compilation (object files) and the executable file (this directory is created automatically by command make release).
- doc includes documentations.
- res is the user directory for data and results.

### 3.3.5 Preparation of input files by the SIMUB generator

Subpackage SIMUB/BB dec allows one to obtain the events with  $B_s^0 \rightarrow J/\psi\phi \rightarrow \mu^+\mu^-K^+K^-$  decays with full physics contents by setting the channel option COPT SI1 in command file BB dec/mak/run [36] and using the decay mechanism option B0SM 1 (B0DM 1) and decay channel option B0SC 1 (B0DC 1) for B0s (B0d) mesons. The format of the SIMUB event is defined by option FRMT. Subpackage SIMUB/BB dec has a mode; Mode Loop==2 to produce events in the format readable by the program BtoVVana. The variable Mode Loop is set in the file BB dec/mak/run by option MODD 2. In this case the format defined by option FRMT is ignored and the events are written in ROOT tree in the format defined in the constructor of class T Loop (subpackage SIMUB/BB dec) in the following way:

```

if(Mode_Loop==2){
hfile= new TFile(fname,"RECREATE"," $B_s^0 \rightarrow J/\Psi\Phi$  or  $B_d^0 \rightarrow J/\Psi K^*$  tree");
tree = new TTree("T"," $B_s^0 \rightarrow J/\Psi\Phi$  decay tree");
tree->Branch("VB",&VB,"x/D:y:z:t:tau");
tree->Branch("PB",&PB,"x/D:y:z:E:M");
tree->Branch("Pa",&Pa,"x/D:y:z:E:M");
tree->Branch("Pa1",&Pa1,"x/D:y:z:E:M");
tree->Branch("Pa2",&Pa2,"x/D:y:z:E:M");
tree->Branch("Pb",&Pb,"x/D:y:z:E:M");
tree->Branch("Pb1",&Pb1,"x/D:y:z:E:M");
tree->Branch("Pb2",&Pb2,"x/D:y:z:E:M");

```

Here fname is the name of the output file defined by option OUTF NAME.root, the branches VB and PB define the secondary 4-vertex of B-decay and 4-momentum of B-meson, branches Pa and Pb define 4-momentum of  $J/\psi$  and  $\phi$  mesons, branches Pa1 and Pa2 define 4-momentum of  $\mu^+$  and  $\mu^-$  mesons, branches Pb1 and Pb2 define 4-momentum of  $K^+$  and  $K^-$  mesons.

### 3.4 ROOT

After many years of experience in developing interactive data analysis systems like PAW[42], it was realized that the growth and maintainability of these products, written in FORTRAN and using 20-year-old libraries, had reached its limits. Although still popular in the physics community, these systems do not scale up to the challenges offered by the next generation particle accelerator, the Large Hadron Collider (LHC), currently under construction at CERN, in Geneva, Switzerland. The expected

amount of data produced by LHC will be of the order of several petabytes (1PB = 1,000,000GB) per year. This is two to three orders of magnitude more than what is being produced by the current generation of accelerators. This was the motivation to build ROOT framework.

ROOT is an object-oriented framework aimed at solving the data analysis challenges of high-energy physics. It was originally designed for particle physics data analysis and contains several features specific to this field, but it is also commonly used in other applications where large amounts of data need to be processed such as astronomy and data mining. It is written in C++ language. It is more user friendly. The ROOT package contains many useful functions that make our analysis comprehensive and easy. Some of the important functions are histogramming and graphing to visualize and analyze distributions and functions, curve fitting and minimization of functionals, statistics tools used for data analysis, matrix algebra, four-vector computations, as used in high energy physics, standard mathematical functions, 3D visualizations (geometry) and interfacing Monte Carlo event generators.

A key feature of ROOT is a data container called tree, with its substructures branches and leaves. ROOT's focus on performance is caused by the amount of data that the Large Hadron Collider's experiments will collect, estimated to several petabytes per year. Physicists are expected to analyze this data using ROOT. Currently ROOT is mainly used in data analysis and data acquisition in high energy physics experiments most current experimental plots and results are obtained using ROOT.

Many particle accelerators use ROOT for the physics analysis e.g. BaBar, CDF,

PHENIX and also future detectors as ALICE, ATLAS, CMS, LHCb. Some important classes that I have used in my code are TVector3, TRotation, TLorentzVector, TLorentzRotation and some histogram classes.

### 3.5 Lorentz Transformation

In physics, the Lorentz transformation relates measurements of spacetime between two different observers, where one observer is in constant motion with respect to the other. Assume there are two observers O and Q, each using their own Cartesian coordinate system to measure space and time intervals. The observer O uses  $(t, x, y, z)$  and Q uses  $(t', x', y', z')$ . In the rest frame of O, the relative velocity of Q is  $v$  along x-axis then the Lorentz transformations for frames in standard configuration are:

$$t' = \gamma \left( t - \frac{vx}{c^2} \right), \quad (3.5.1)$$

$$x' = \gamma (x - vt), \quad (3.5.2)$$

$$y' = y, \quad (3.5.3)$$

$$z' = z, \quad (3.5.4)$$

where  $\gamma = \frac{1}{\sqrt{1-(v^2/c^2)}}$  is called the Lorentz factor.

A boost in a general direction can be parameterized with three parameters which can be taken as the components of a three vector  $\mathbf{b}=(\beta_x, \beta_y, \beta_z)$ . With  $\mathbf{x}=(x, y, z)$  and

$\gamma = \frac{1}{\sqrt{1-\beta^2}}$  ( $\beta$  being the module of vector  $b$  as  $\beta = |b|$ ), an arbitrary active Lorentz boost transformation (from the moving frame to the rest frame) can be written as:

$$r = r' + \frac{(\gamma - 1)}{\beta^2}(b \cdot r')b + \gamma b t' \quad (3.5.5)$$

$$t = \gamma(t' + b r') \quad (3.5.6)$$

$$\begin{bmatrix} ct \\ x \\ y \\ z \end{bmatrix} = \begin{bmatrix} 1 + \gamma' \beta_x^2 & \gamma' \beta_x \beta_y & \gamma' \beta_x \beta_z & \beta_x \gamma \\ \gamma' \beta_y \beta_x & 1 + \gamma' \beta_y^2 & \gamma' \beta_y \beta_z & \beta_y \gamma \\ \gamma' \beta_z \beta_x & \gamma' \beta_z \beta_y & 1 + \gamma' \beta_z^2 & \beta_z \gamma \\ \beta_x \gamma & \beta_y \gamma & \beta_z \gamma & \gamma \end{bmatrix} \begin{bmatrix} ct' \\ x' \\ y' \\ z' \end{bmatrix} \quad (3.5.7)$$

where  $\gamma' = \frac{(\gamma-1)}{\beta^2}$

# Chapter 4

## Results and Discussion

### 4.1 Invariant Mass

The Invariant Mass is a scalar quantity, it is a Lorentz Invariant, hence its values is same in all frames of references. If a particle of mass  $M$  decays to  $n$  objects, the invariant mass of the  $n$  objects will be  $M$  as given by relation below:

$$M^2 = p_\mu p^\mu = \sum_{i=1}^n E_i^2 - \sum_{i=1}^n p_i^2 \quad (4.1.1)$$

where  $p_\mu$  is four momentum of decaying particle, while  $E_i$ ,  $p_i$  are energy and 3-momentum of daughter particle.

From the above formulation the invariant mass of  $B_s^0$  can be determined by the energy and momenta components of  $J/\psi$  and  $\phi$ .

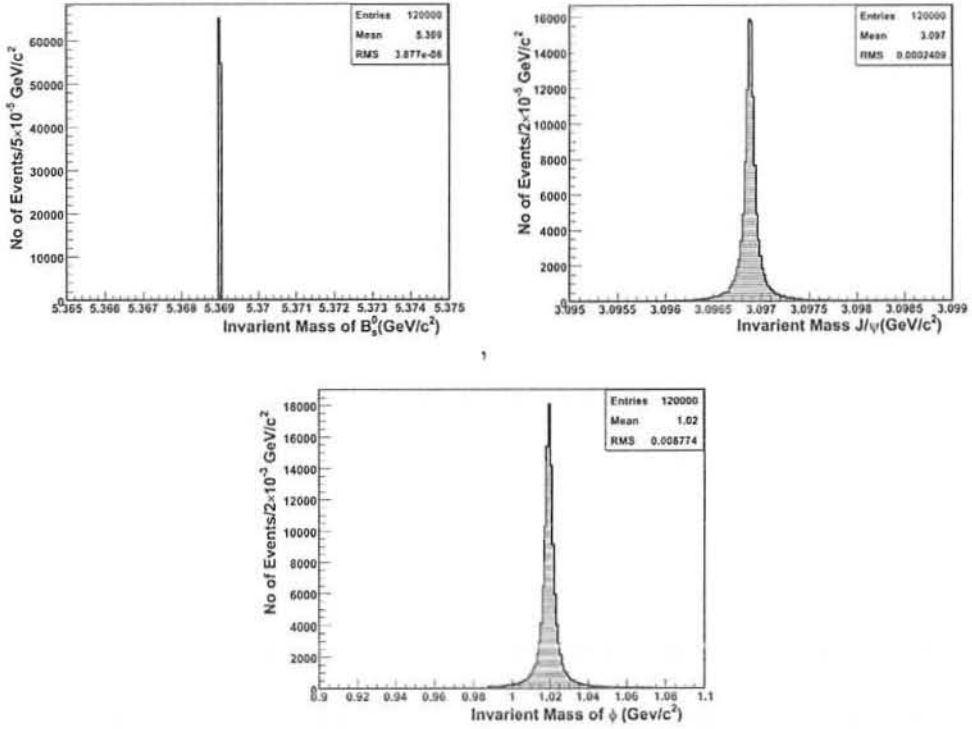


Figure 4.1: Invariant Mass of  $B_s^0$ ,  $J/\psi$  and  $\phi$ .

From the current study we have plotted the invariant mass distribution of  $B_s^0, J/\psi$  and  $\phi$  and found their mean mass values to be at  $5.369 \text{ GeV}/c^2$ ,  $3.097 \text{ GeV}/c^2$ ,  $1.02 \text{ GeV}/c^2$  respectively. The plots are shown in Fig. 4.1.

## 4.2 Opening Angle

The opening angle is the angle between the daughter particles when they decay in Lab frame.

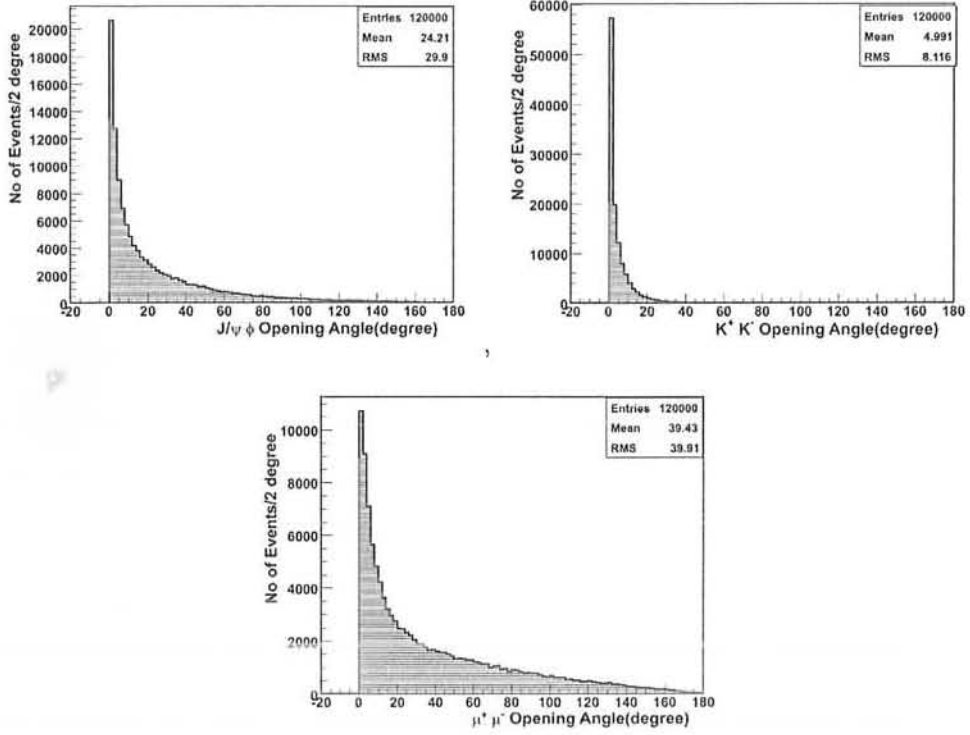


Figure 4.2: Opening Angle of  $B_s^0$ ,  $J/\psi$  and  $\phi$ .

The opening angle between the daughter particles decreases with increasing the Boost of the parent particle, and mathematically its expression is given by

$$\Theta = \text{Cos}^{-1} \left( \frac{P_{X_1} \cdot P_{X_2} + P_{Y_1} \cdot P_{Y_2} + P_{Z_1} \cdot P_{Z_2}}{\sqrt{P_{X_1}^2 + P_{Y_1}^2 + P_{Z_1}^2} \sqrt{P_{X_2}^2 + P_{Y_2}^2 + P_{Z_2}^2}} \right) \quad (4.2.1)$$

In our study we plotted the opening angles between  $J/\psi$  and  $\phi$ ,  $\mu^+$  and  $\mu^-$  and  $K^+$  and  $K^-$  and found their mean values to be 24.21 degrees, 39.43 degrees, 4.991 degrees when they decay from  $B_s^0$ ,  $J/\psi$  and  $\phi$  respectively. The plots are shown in Fig. 4.2.



### 4.3 Total Momentum

Total Momentum of the particles can be calculated from its 3-momentum components as

$$p = \sqrt{p_x^2 + p_y^2 + p_z^2} \quad (4.3.1)$$

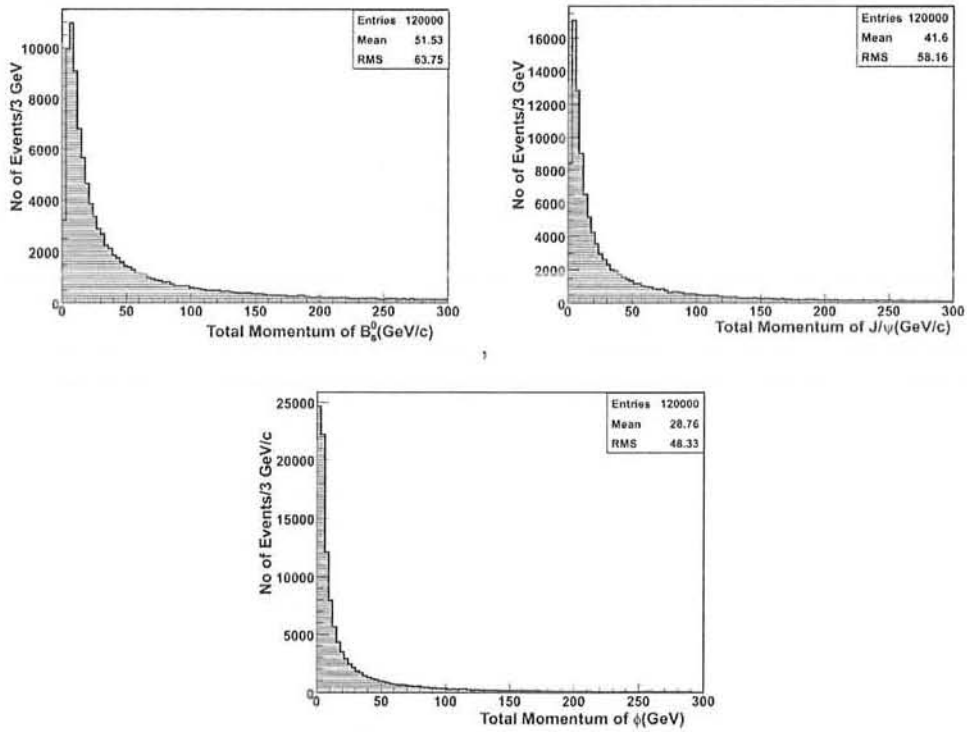


Figure 4.3: Total Momentum of  $B_s^0$ ,  $J/\psi$  and  $\phi$ .

In the Fig. 4.3 and Fig. 4.4 the plots of total momentum of  $B_s^0$ ,  $J/\psi$  and  $\phi$  and  $\mu^+$ ,  $\mu^-$ ,  $K^+$  and  $K^-$  respectively are shown. These plots show that most of the events

are produced at the low momenta while small number of events are produced at higher values of momenta.

The means values of total momenta for  $B_s^0$ ,  $J/\psi$ ,  $\phi$ ,  $\mu^+$ ,  $\mu^-$ ,  $K^+$  and  $K^-$  are 51.53, 41.6, 28.76, 26.09, 26.4, 18.37 and 18.25 in units of GeV/c. The plots show that daughter particles have smaller ranges than that of the parent particles.

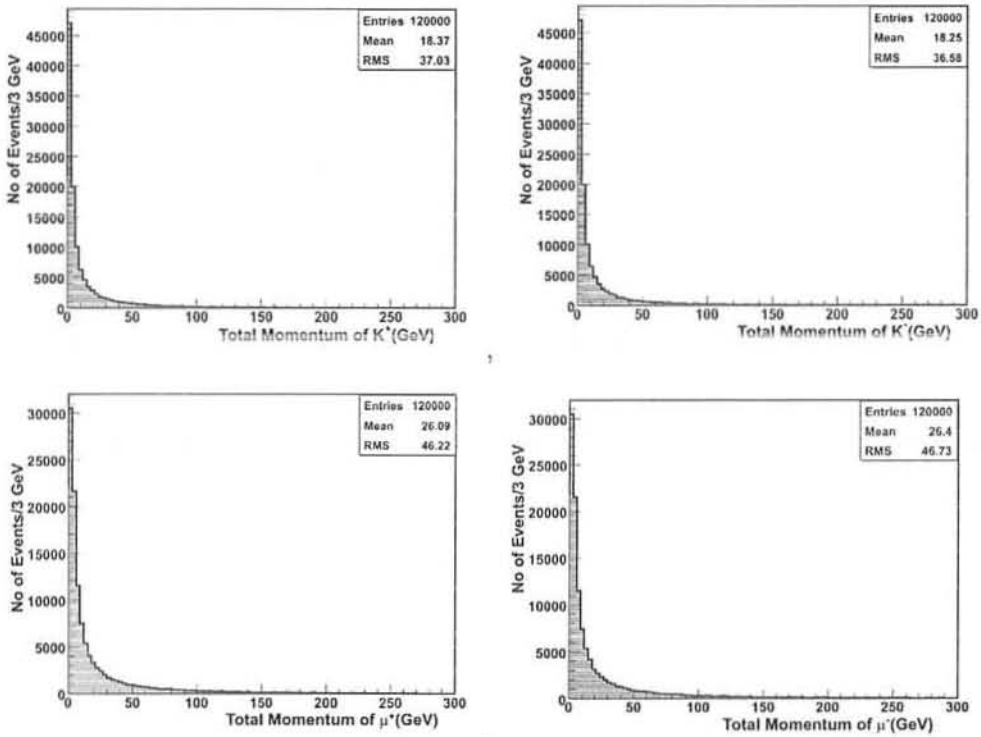


Figure 4.4: Total Momentum of  $\mu^+$ ,  $\mu^-$ ,  $K^+$  and  $K^-$ .

## 4.4 Transverse Momentum

The transverse momentum of the particles in the detector is the component of momentum transverse to z-axis (direction of beam) and its expression is given mathematically as

$$p_T = \sqrt{p_x^2 + p_y^2} \quad (4.4.1)$$

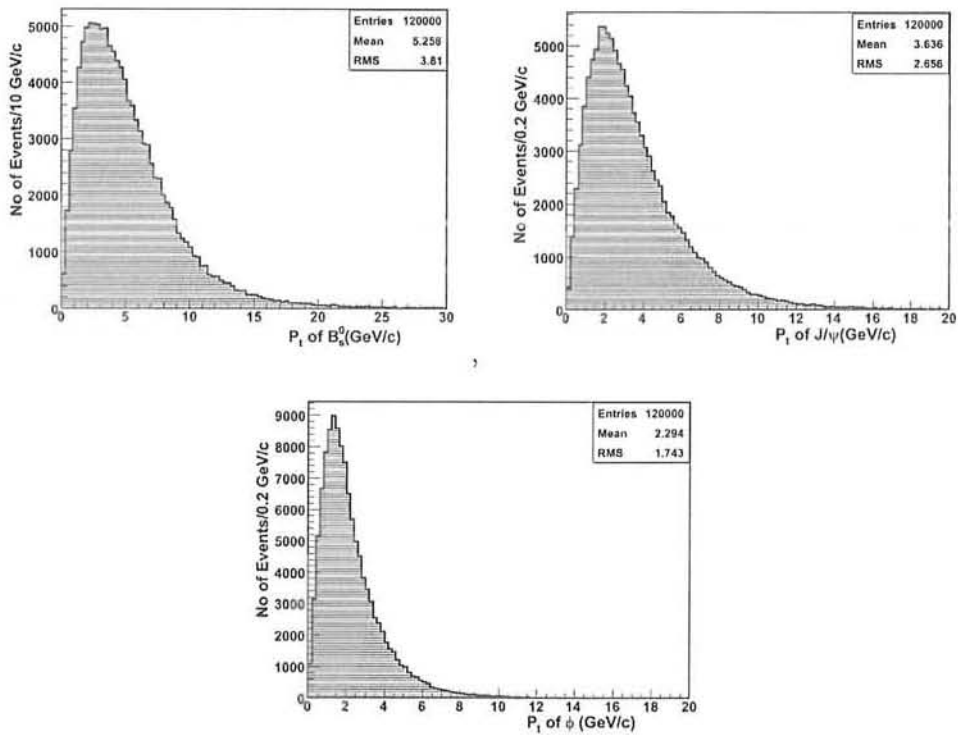


Figure 4.5: Transverse Momentum of B<sub>s</sub><sup>0</sup>, J/ψ and φ.

#### 4.4.1 Transverse Momentum of $B_s^0$ , $J/\psi$ and $\phi$

The transverse momenta of  $B_s^0$ , has a distribution with a long tail on the higher end and a mean of  $5.26\text{GeV}/c$ . The plot also shows that the transverse momenta of  $B_s^0$ , varies from 0 to nearly  $25\text{GeV}/c$ .

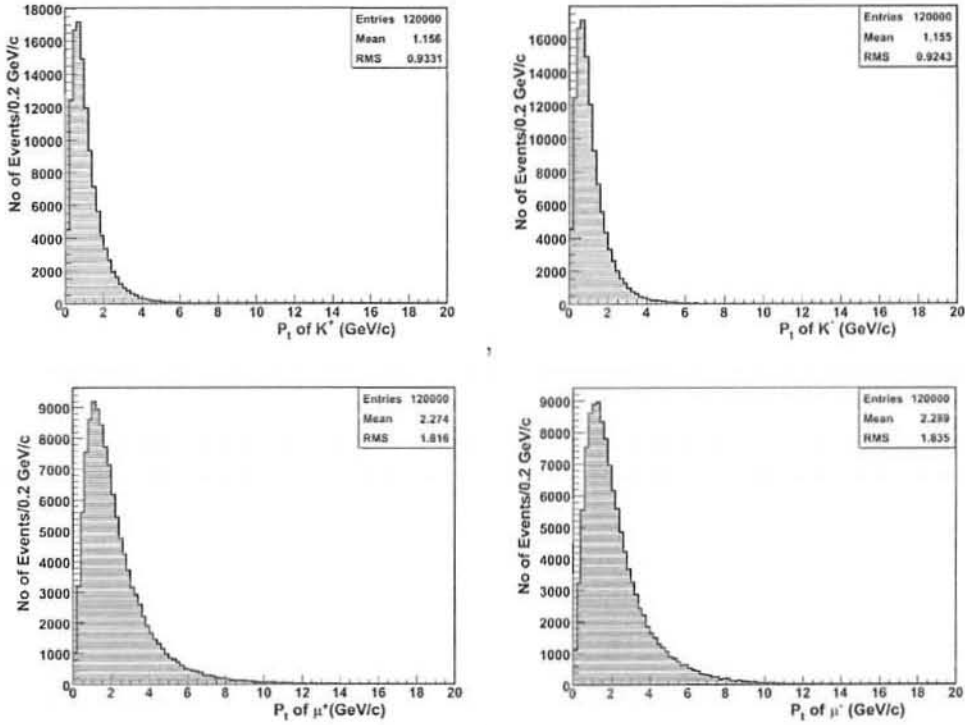


Figure 4.6: Transverse Momentum of  $\mu^+$ ,  $\mu^-$ ,  $K^+$  and  $K^-$ .

Hence we can have  $B_s^0$ , produced along beam as well as in the barrel. Low transverse momenta  $B_s^0$ , are produced at higher eta values and vice versa. Transverse Momentum of  $J/\psi$  and  $\phi$  are similar in shape to that of  $B_s^0$ , but with a mean of  $3.64\text{GeV}/c$  and  $18\text{GeV}/c$  respectively. And the range lies from 0 to nearly  $20\text{GeV}/c$

and 12GeV/c for  $J/\psi$  and  $\phi$  respectively. Since  $J/\psi$  and  $\phi$  are produced from  $B_s$ , the mean and range is smaller than that of  $B_s^0$ , as expected. The plots are shown in Fig. 4.5.

#### 4.4.2 Transverse Momentum of $\mu^+$ , $\mu^-$ , $K^+$ and $K^-$

The distribution of transverse momenta of  $\mu^+$ ,  $\mu^-$ ,  $K^+$  and  $K^-$  are similar in shape to that of  $B_s^0$ , but with a mean of 2.27GeV/c, 2.29GeV/c, 1.16GeV/c and 1.16GeV/c and the range lies from 0 to nearly 11GeV/c, 11GeV/c, 6GeV/c and 6GeV/c respectively. Since  $\mu^+$  and  $\mu^-$  are produced from  $J/\psi$ , the mean and range is smaller than that of  $J/\psi$  as expected and similarly as  $K^+$  and  $K^-$  are produced from  $\phi$ , the mean and range is smaller than that of  $\phi$ . The plots are shown in Fig. 4.6.

### 4.5 Total Energy

The total energy of  $B_s^0$ ,  $J/\psi$ ,  $\phi$ ,  $\mu^+$ ,  $\mu^-$ ,  $K^+$  and  $K^-$  is 52.44, 42.07, 28.86, 26.09, 26.4, 18.42 and 18.3 in the units of GeV respectively as shown by the following distribution in Fig. 4.7 and Fig. 4.8.

The range of total energy is larger for parent particles than that of daughter particles.

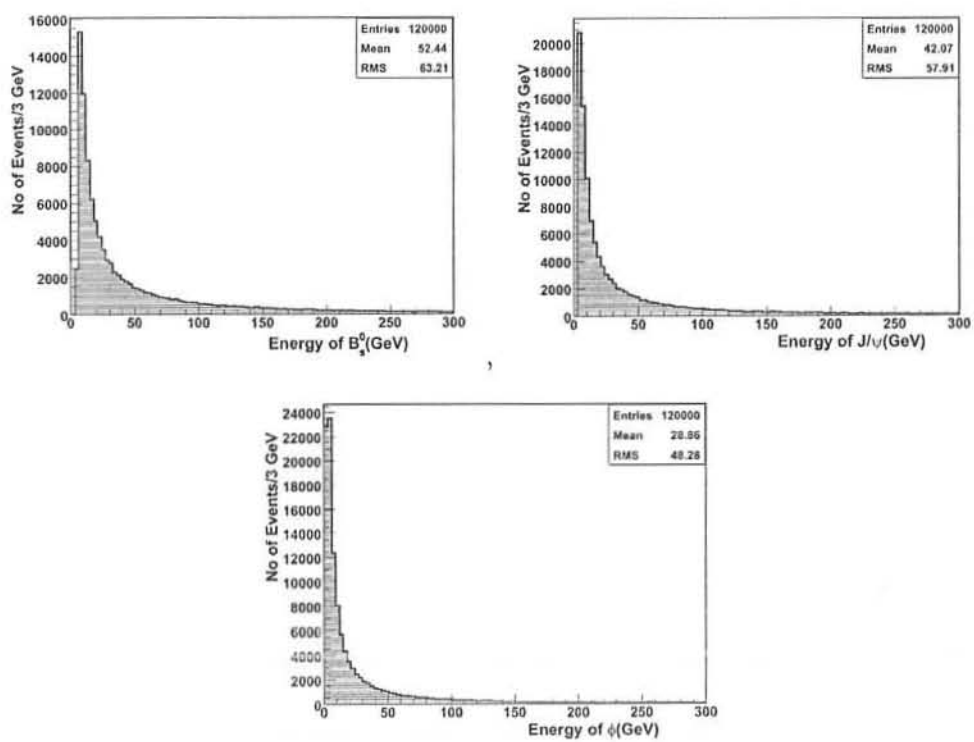


Figure 4.7: Total Energy of  $B_s^0$ ,  $J/\psi$  and  $\phi$ .

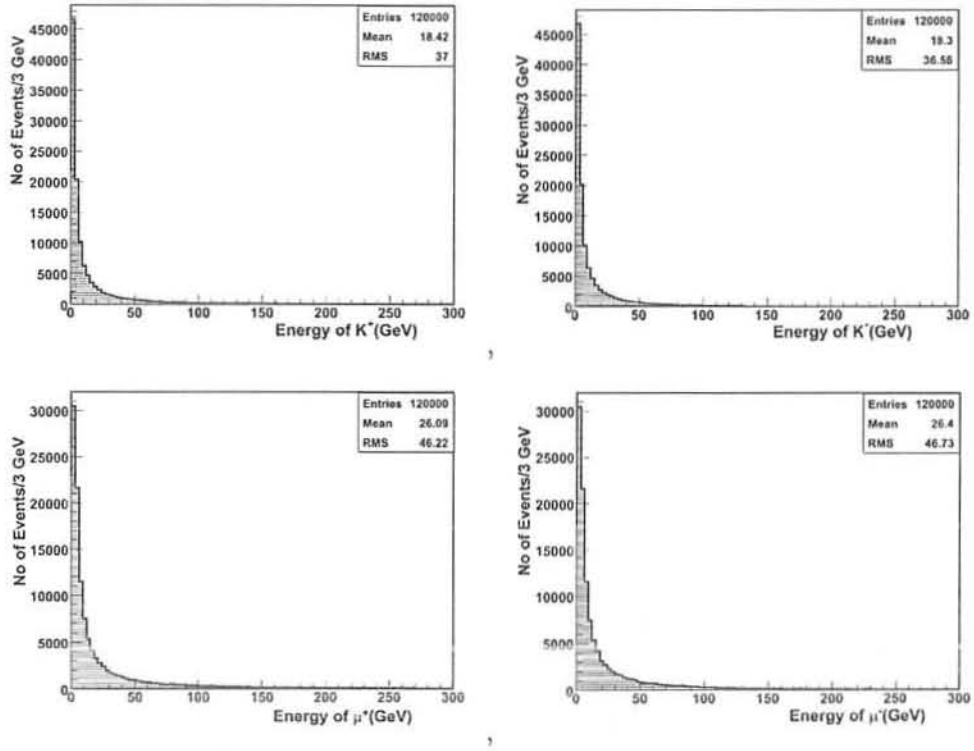


Figure 4.8: Total Energy of  $\mu^+$ ,  $\mu^-$ ,  $K^+$  and  $K^-$ .

## 4.6 Transverse Energy

The transverse energy of particles is related to the total energy mathematically as follows:

$$E_T = E \sin\theta$$

The means values of transverse energy for  $B_s^0$ ,  $J/\psi$ ,  $\phi$ ,  $\mu^+$ ,  $\mu^-$ ,  $K^+$  and  $K^-$  are 5.752, 6.078, 7.19, 8.701, 8.693, 7.22 and 7.223 in units of GeV respectively. The plots are

shown in Fig. 4.9 and Fig. 4.10.

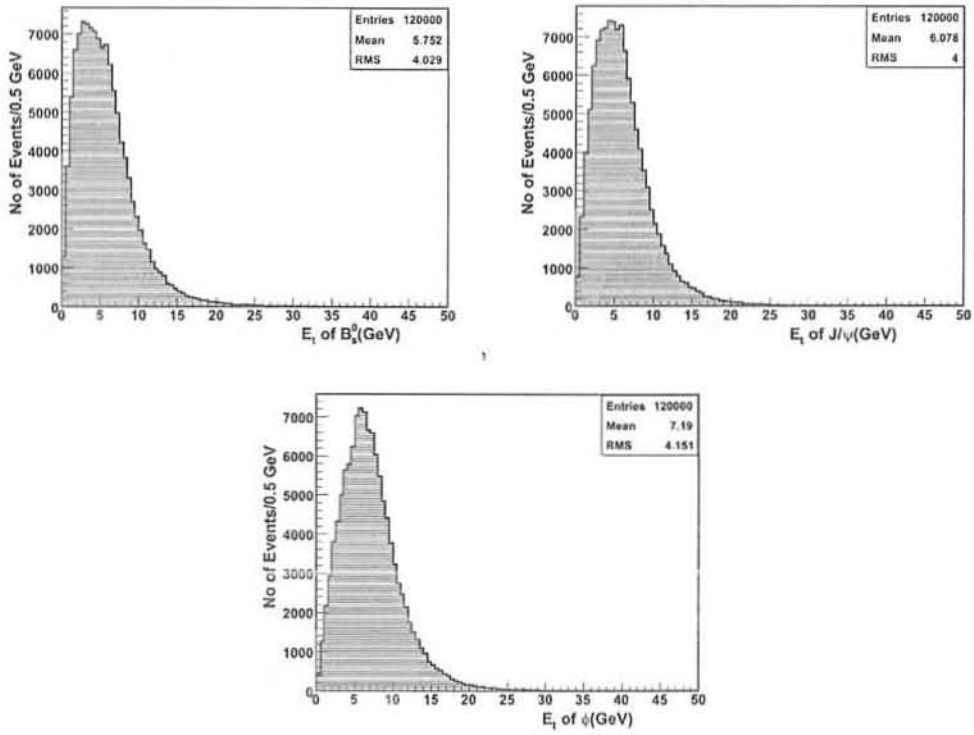


Figure 4.9: Transverse Energy of  $B_s^0$ ,  $J/\psi$  and  $\phi$ .

The transverse energy of the particles is smaller than the total energy as is obvious from the distribution.



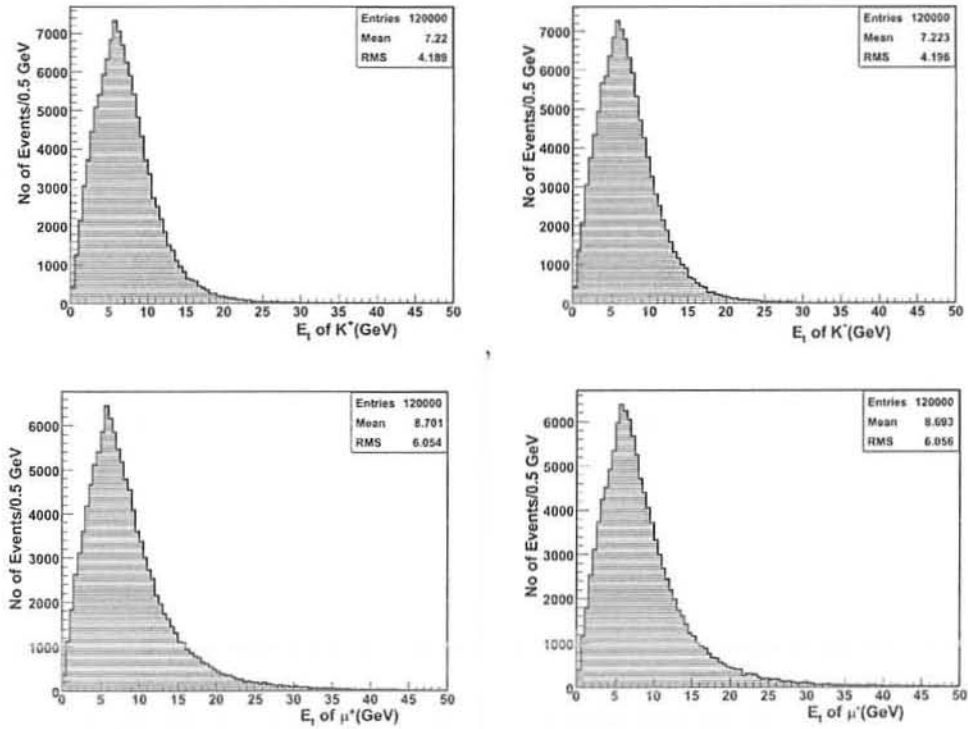


Figure 4.10: Transverse Energy of  $\mu^+$ ,  $\mu^-$ ,  $K^+$  and  $K^-$ .

## 4.7 Pseudorapidity

In experimental particle physics, Pseudorapidity,  $\eta$ , is a commonly used spatial coordinate describing the angle of a particle relative to the beam axis. Its mathematical expression is defined as:

$$\eta = -\ln \left( \tan \frac{\theta}{2} \right) \quad (4.7.1)$$

where  $\theta$ , is the polar angle relative to the beam axis. Some values of pseudorapidity

corresponding to polar angle  $\theta$  are shown in Table 4.1.

Table 4.1: Values of pseudorapidity corresponding to polar angle  $\theta$

$\theta(\text{degrees})$	0	5	10	20	30	45	60	80	90
$\eta$	infinite	3.13	2.44	1.74	1.31	0.88	0.55	0.175	0

In hadron collider physics, the pseudorapidity is preferred over the polar angle  $\theta$  because, loosely speaking, particle production is constant as a function of pseudorapidity.

#### 4.7.1 Pseudorapidity of $B_s$ , $J/\psi$ , $\phi$

The pseudorapidity of  $B_s^0$ ,  $J/\psi$ ,  $\phi$  shows two obvious peaks pointing to the fact that they are mostly produced at eta values 2 to 4 corresponding to outer barrel of the detector. The number of these particles produced normal to beam direction are less as compared to those produced in the outer barrel. The plots are shown in Fig. 4.11.

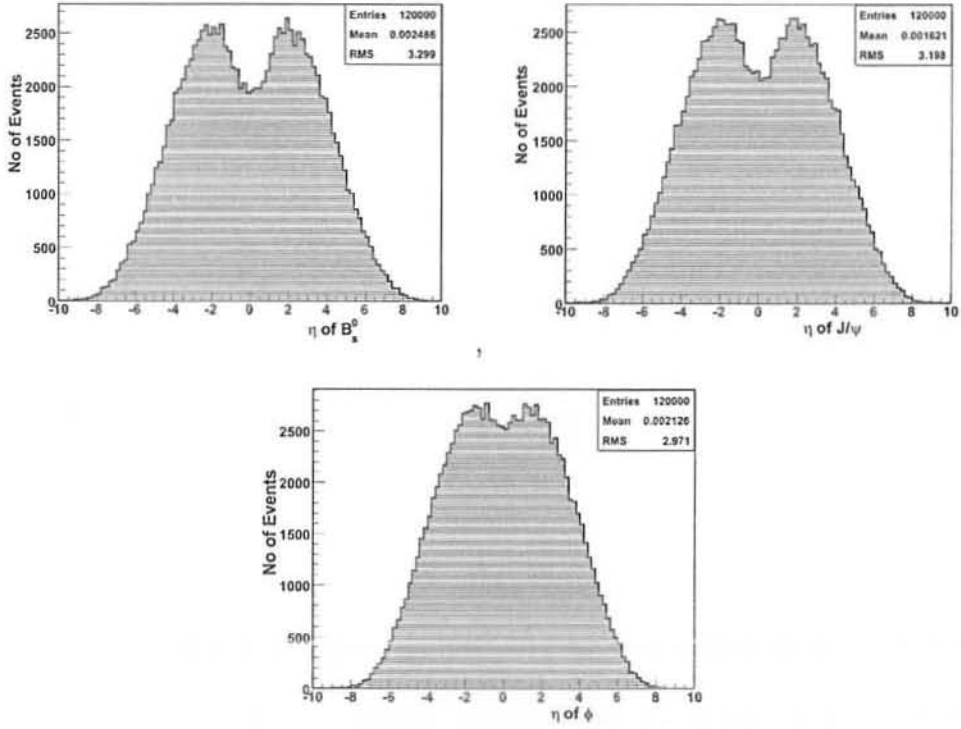


Figure 4.11: Pseudorapidity of  $B_s^0$ ,  $J/\psi$  and  $\phi$ .

#### 4.7.2 Pseudorapidity of $\mu^+$ , $\mu^-$

The pseudorapidity of  $\mu^+$ ,  $\mu^-$  shows only one peak pointing to the fact that they are mostly produced normal to beam direction and their number produced decreases as we go towards the endcap. We can have more muons (mass  $\sim 106 \text{ MeV}/c^2$ ) in the transverse direction since they are produced from  $J/\psi$  with higher momenta with a mean of  $2.29 \text{ GeV}/c$ . The plots are shown in Fig. 4.12.

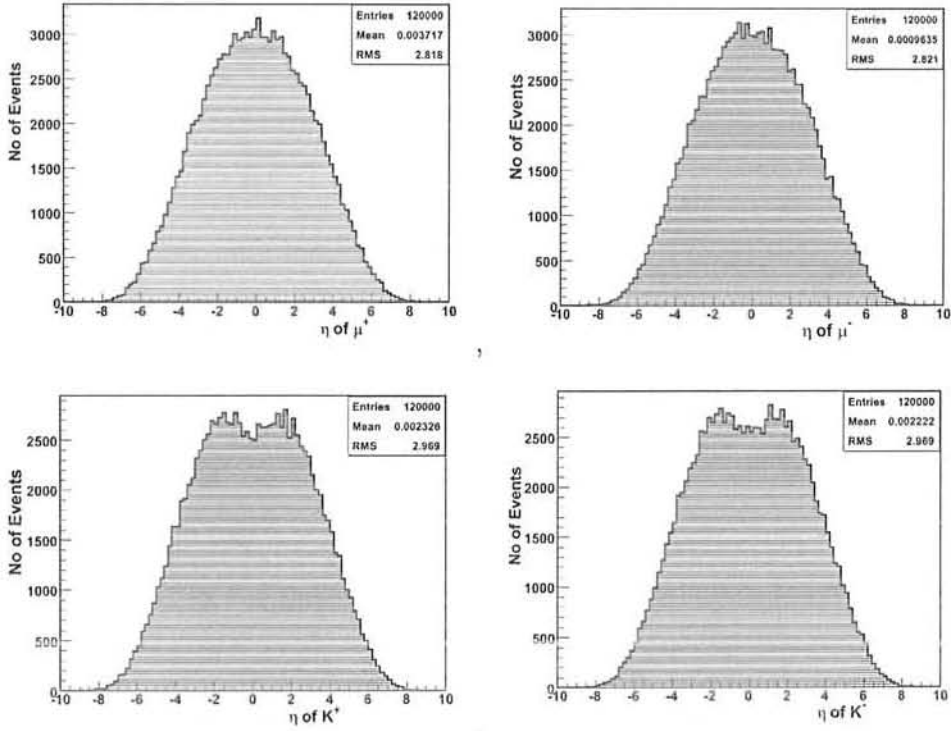


Figure 4.12: Pseudorapidity of  $\mu^+$ ,  $\mu^-$ ,  $K^+$  and  $K^-$ .

### 4.7.3 Pseudorapidity of $K^+$ , $K^-$

The pseudorapidity of  $K^+$ ,  $K^-$  shows two peaks pointing to the fact that they are mostly produced at eta values 2-4 corresponding to outer barrel of the detector. The number produced normal to beam direction is less as compared to those produced in the outer barrel. The pseudorapidity distribution for kaons (mass  $\approx 490 \text{ MeV}/c^2$ ) is not similar to that of muons since they are produced at relatively lower momenta with a mean of  $1.16 \text{ GeV}/c$ . The plots are shown in Fig. 4.12.

## 4.8 Polar Angle

Polar Angle is the angle of the particles with the beam axis. The plots show that most of the particles are produced along beam direction. The plots of the polar angle distribution for  $B_s^0$ ,  $J/\psi$  and  $\phi$  are shown in Fig. 4.13,

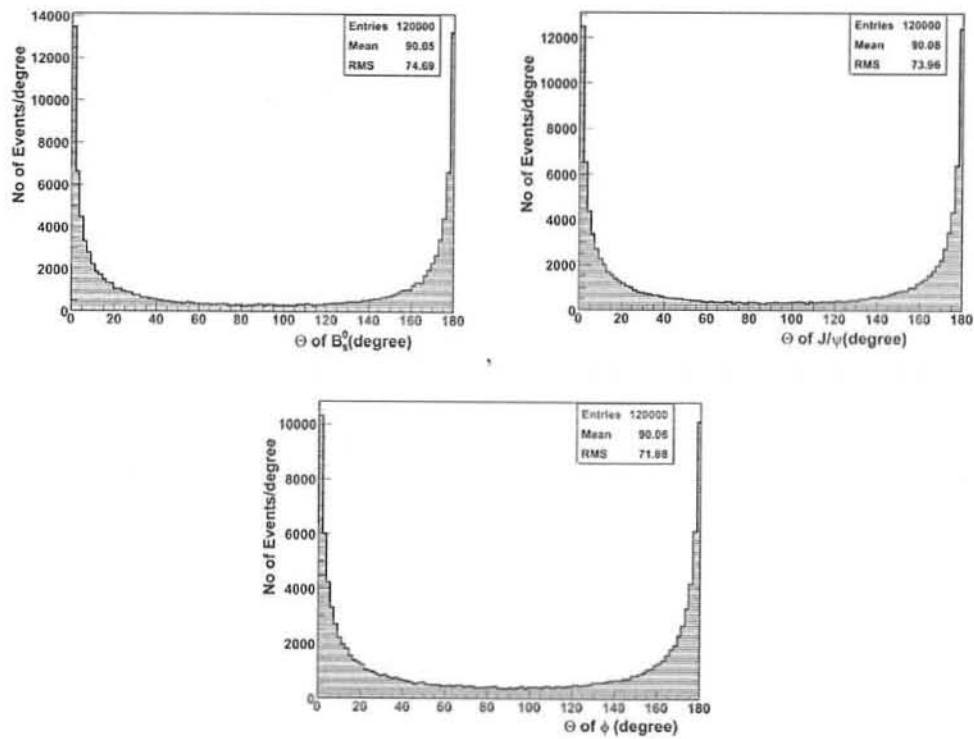


Figure 4.13: Polar Angle of  $B_s^0$ ,  $J/\psi$  and  $\phi$ .

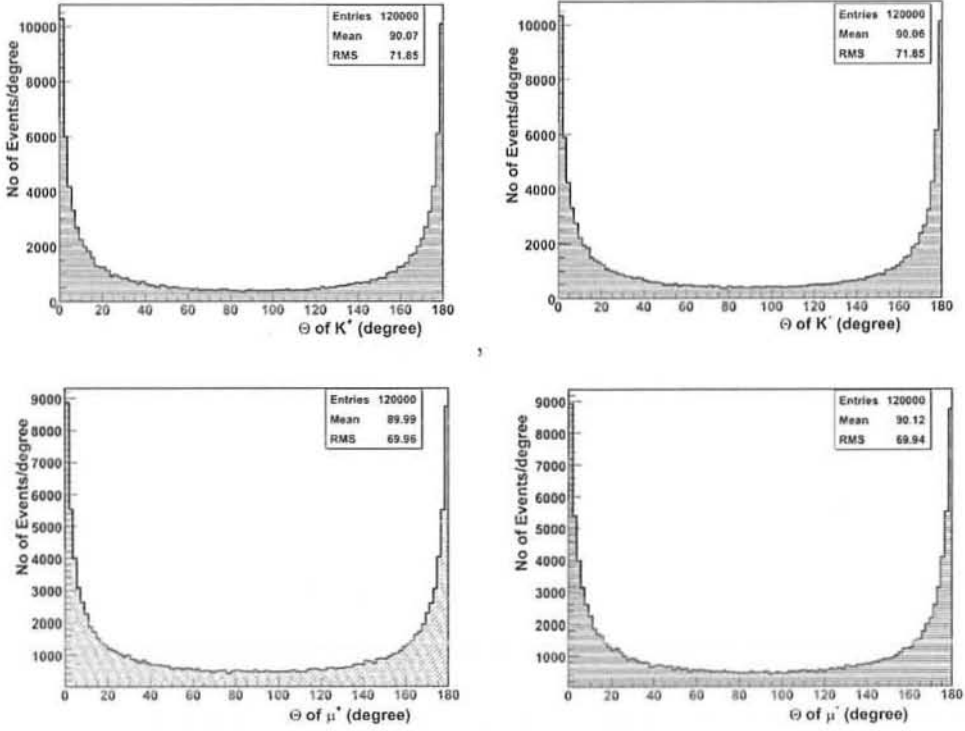


Figure 4.14: Polar Angle of  $\mu^+$ ,  $\mu^-$ ,  $K^+$  and  $K^-$ .

and those for  $\mu^+$ ,  $\mu^-$ ,  $K^+$  and  $K^-$  are shown in Fig. 4.14.

## 4.9 Boost

Fig. 4.15 and Fig. 4.16 show the boost for particles involved in our channel. Boost is defined as the product of Lorentz factor gamma and velocity beta i.e  $\gamma\beta$ . Mathematically it turns out to be equal to the ratio of momentum to the rest mass of a particle. It is more convenient to plot this factor in log scale so we write:

$$Boost = \ln \left( \frac{\sqrt{P_{X_1}^2 + P_{Y_1}^2 + P_{Z_1}^2}}{M} \right) \quad (4.9.1)$$

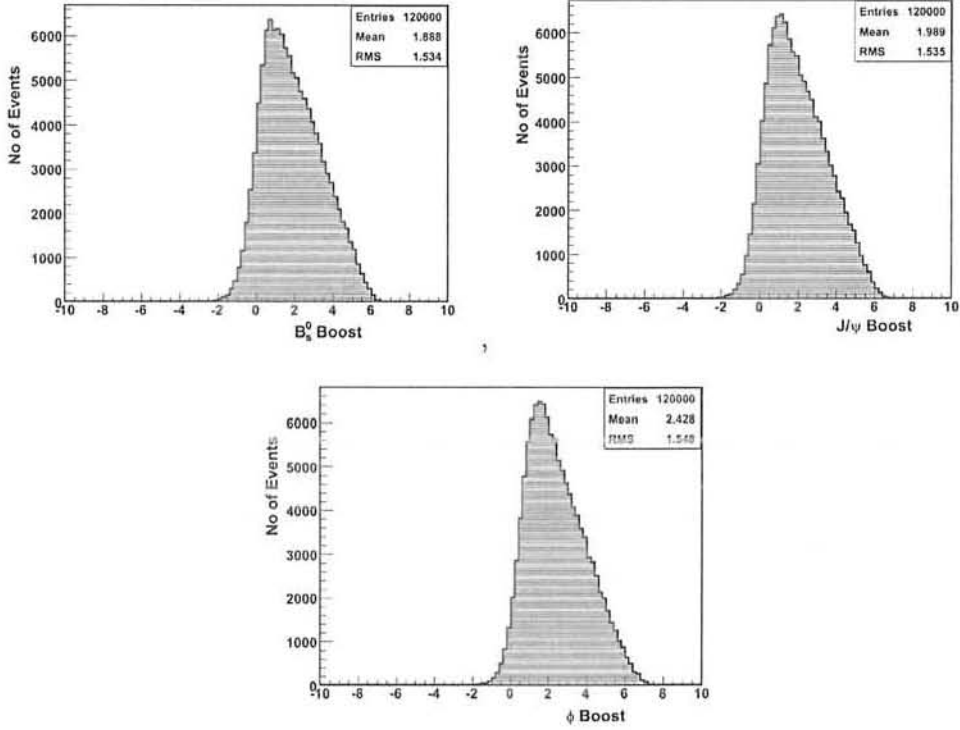


Figure 4.15: Boost of  $B_s^0$ ,  $J/\psi$  and  $\phi$ .

The Boost is always positive. Boost for  $B_s^0$ ,  $J/\psi$  and  $\phi$  ranges from decimal values (corresponding to particles produced at almost rest) to 200-300 (corresponding to particles produced at higher momentum).  $\mu^+$ ,  $\mu^-$ ,  $K^+$  and  $K^-$  are produced with relatively higher boost ranging upto 20000 and 1000 respectively.

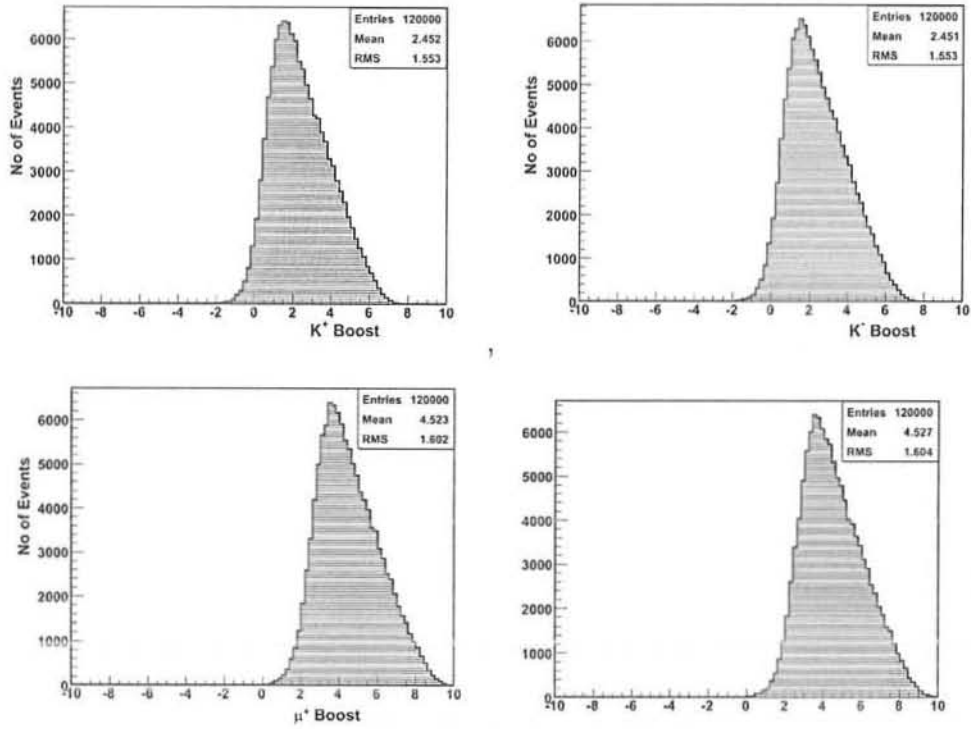


Figure 4.16: Boost of  $\mu^+$ ,  $\mu^-$ ,  $K^+$  and  $K^-$ .

## 4.10 Helicity Angles

### 4.10.1 Distribution of $\text{Cos } \Theta_{\mu^+}$

The plot shows the distribution of the polar angle for  $\mu^+$ . The positive z-axis is defined as the direction of flight of  $\phi$  in the rest frame of  $B_s^0$ . This frame is also known as the helicity frame. In the helicity frame most muons are produced normal to the z-axis (direction of flight of  $J/\psi$  and  $\phi$ ). The plot is shown in the Fig. 4.17.



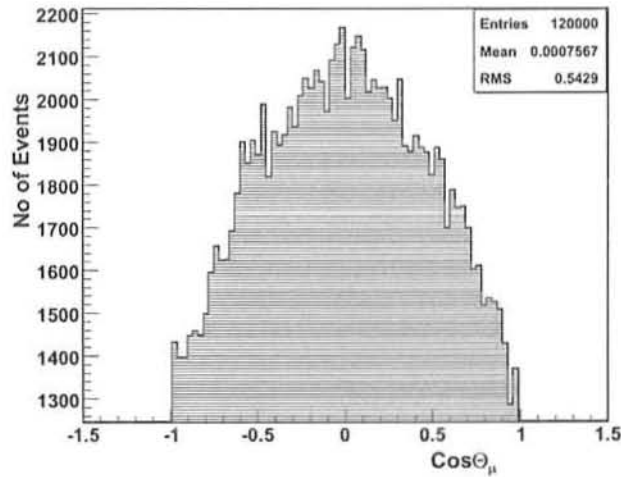


Figure 4.17: Distribution of  $\text{Cos } \Theta_{\mu^+}$

#### 4.10.2 Distribution of $\text{Cos } \Theta_{K^+}$

The plot shows the distribution of the polar angle for  $K^+$ . The positive z-axis is same. In the helicity frame most kaons are produced along z-axis (i.e. parallel to the direction of flight of  $J/\psi$  and  $\phi$ ). The plot is shown in Fig. 4.18.

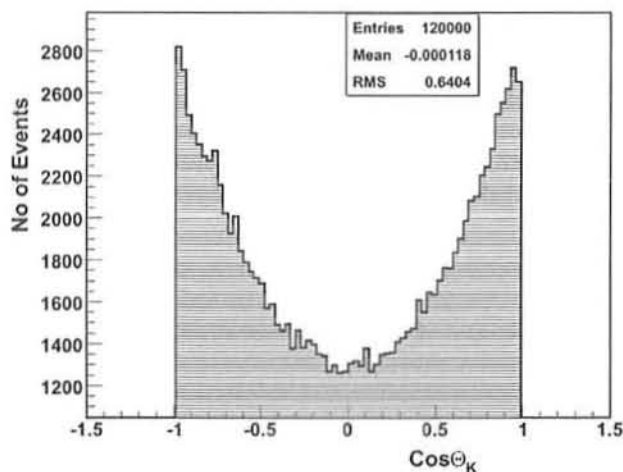
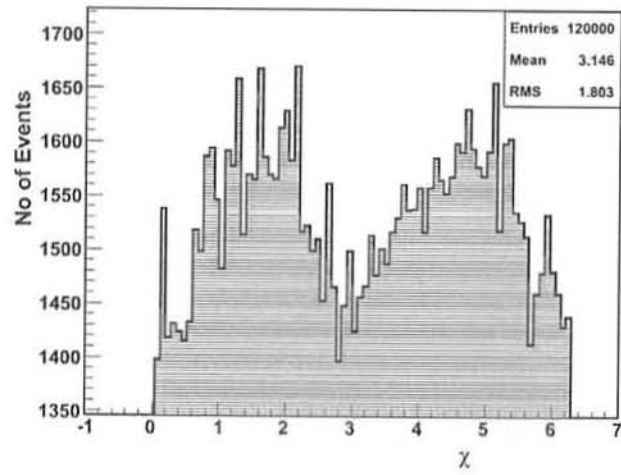


Figure 4.18: Distribution of  $\text{Cos } \Theta_{K^+}$

### 4.10.3 Distribution of $\chi$

This plot shows the difference of azimuthal angle of muons and kaons for each event. The azimuthal angle for muons and kaons is not useful as x-axis is defined arbitrarily but the difference shown by the following plot gives useful information. The plot is shown in the Fig. 4.19.

Figure 4.19: Distribution of  $\chi$

# Conclusion

The LHC at CERN will be the largest  $b$ -factory ever built. The decay  $B_s^0 \rightarrow J/\psi \phi \rightarrow \mu^+ \mu^- K^+ K^-$  is chosen as a benchmark channel since it is representative of exclusive B physics studies. It allows to study the capability of CMS to identify, select and fully reconstruct the decay of the  $B_s^0$ , which presents a significant challenge due to its relatively low momentum and high background.

We performed the generator level study of this channel using a specialized  $b\bar{b}$  generator called SIMUB and BtoVVana. The generator level distributions of 120000 events of  $B_s^0 \rightarrow J/\psi \phi \rightarrow \mu^+ \mu^- K^+ K^-$  were studied, in particular their helicity angle distributions which were not possible to be study using only PYTHIA, QQ and CMSSW. The following distributions are generated for each particle involved in the decay : Invariant Mass, Opening Angle, Total Momentum, Transverse Momentum, Total Energy, Transverse Energy, Pseudorapidity, Polar Angle, Boost and Helicity Angles. These distributions help to constraint different variables such as transverse momentum, transverse energy, pseudorapidity etc. at the reconstruction level. Hence they are useful for the analysis of real data when the detector will become operational.

# Bibliography

- [1] FERMILAB-Conf-97/432
- [2] <http://pdg.lbl.gov/2006/listings/q005.pdf>
- [3] G. Altarelli, G. Parisi, "Asymptotic freedom in parton language," Nucl. Phys.B 126 (1977) 298.
- [4] Particle Data Group, "The Cabbibo-Cobayashi-Moskawa Quark-Mixing Matrix," Phys. Lett. B 592 (2004), no. 1-4, 130
- [5] G. Altarelli, G. Parisi, "Asymptotic freedom in parton language," Nucl. Phys.B 126 (1977) 298
- [6] E. Norrbin, T. Sjostrand , "Production and Hadronization of Heavy Quarks." arXiv:hep-ph/0005110, 2000
- [7] S. Alekhin et al., "QCD," in Proceedings of the Workshop on Standard Model Physics (and more) at the LHC, CERN 2000-004. 2000
- [8] J. Baines et al., "B Production," in Proceedings of the Workshop on Standard Model Physics (and more) at the LHC, CERN 2000-004. 2000
- [9] L. Wolfenstein, Parametrization of the Kobayashi-Maskawa Matrix," Phys. Rev. Lett. 51 (1983), no. 21, 1945

- [24] CMS Collaboration, "The Compact Muon Solenoid Technical Proposal", CERN/LHCC 94-38, LHCC/P1, 15 December 1994.
- [25] CMS Collaboration, "The Compact Muon Solenoid Letter of Intent", CERN/LHCC 92-3, LHCC/II, 1 October 1992.
- [26] CMS Collaboration, CMS Design Team, "CMS: The Magnet Project Technical Design Report", CERN/LHCC 97-10, CMS TDR 1, 2 May 1997
- [27] CMS Collaboration, "CMS: The Tracker Project Technical Design Report", CERN/LHCC 98-06, CMS TDR 5, 15 April 1998
- [28] CMS Collaboration, "CMS: The Electromagnetic Calorimeter Project Technical Design Report", CERN/LHCC 97-33, CMS TDR 4, 15 December 1997
- [29] CMS Collaboration, "CMS: The Hadron Calorimeter Project Technical Design Report", CERN/LHCC 97-31, CMS TDR 2, 20 June 1997
- [30] CMS Collaboration, "CMS: The Muon Project Technical Design Report", CERN/LHCC 97-32, CMS TDR 3, 15 December 1997
- [31] RD5 Collaboration, Nucl. Instrum. Meth., A336 (1993) 91-97, Bunch Crossing Identification at LHC Using a Mean Timer Technique
- [32] CMS Collaboration, "CMS: The Trigger and Data Acquisition Project, Volume I: The Level-1 Trigger Technical Design Report", CERN/LHCC 2000-038, CMS TDR6.1, 15 December 2000
- [33] CMS Collaboration, "CMS: The Trigger and Data Acquisition Project, Volume II: Data Acquisition and High-Level Trigger Technical Design Report", CERN/LHCC 02-26, CMS TDR 6.2, 15 December 2002
- [34] Ref: <https://twiki.cern.ch/twiki/bin/view/CMS/WorkBookCMSExperiment>